Chinese Chemical Letters 33 (2022) 3657–3671

Contents lists available at ScienceDirect

Chinese Chemical Letters

journal homepage: www.elsevier.com/locate/cclet

Bimetallic two-dimensional materials for electrocatalytic oxygen evolution

Xiaojie Li, Qi Hu, Hengpan Yang, Tao Ma, Xiaoyan Chai, Chuanxin He*

College of Chemistry and Environmental Engineering, Shenzhen University, Shenzhen 518060, China

ARTICLE INFO

Article history:
Received 20 August 2021
Revised 11 October 2021
Accepted 1 December 2021
Available online 5 December 2021

Keywords:
Bimetal/bimetallic
Two-dimensional/2D
Oxygen evolution
Electrocatalytic
MOF
LDH

ABSTRACT

Electrocatalytic oxygen evolution reaction (OER) is one of the important half reactions of electrocatalytic water splitting. However, the slow kinetic process involving four-electron transfer severely limits its reaction efficiency, which in turn limits the overall electrocatalytic hydrolysis efficiency. In order to improve the activity of the electrocatalytic OER, researchers mainly update the catalyst from three aspects, that is, increase the conductivity of the electrocatalyst, and the quantity and quality of active sites. Two-dimensional (2D) engineering can effectively reduce the resistance of the materials and greatly increase the number of electrochemically active sites, while heterometal doping, or the bimetal strategy, can improve the quality of active sites *via* changing the electronic structure of the material. Thus, the combination of the two can enhance the activity of electrocatalytic OER in all three aspects: conductivity, number and quality of active sites. However, there is currently no review on this topic. Therefore, in this review, we summarize the application of bimetallic 2D materials in electrocatalytic OER from four aspects: the structure, synthesis strategy, catalytic efficiency, and reaction mechanism.

1. Introduction

Sustainability and environmental friendliness have become the two major themes of energy issues in the world today [1–7]. Hydrogen energy, which is most in line with these two themes, has continuously aroused researchers' attention in the past decades [8–14]. The electrocatalytic hydrogen evolution reaction (HER) *via* water splitting that can be coupled with photovoltaic cells is undoubtedly one of the hydrogen production methods that best meet these two themes. In this reaction, HER is only one of the half-reactions. The other half is the electrocatalytic oxygen evolution reaction (OER), also known as electrocatalytic water oxidation [15–20]. OER involves a four-electron transfer and its kinetic speed is quite slow, much slower than the opposite half-reaction, HER [21–26]. As a result, the rate of overall electrocatalytic water splitting is controlled by the rate of electrocatalytic water oxidation. Thus, solving the problem of slow kinetic speed of OER means that the reaction rate of the entire electrocatalytic water splitting can be increased, thereby increasing HER efficiency. Similar to HER in water splitting, the anode reaction of electrocatalytic CO_2 reduction (CO_2RR) is also an OER process, so in CO_2RR, OER is expected to have good performance as well [27–30]. Besides, in rechargeable metal-air batteries, the anode of the charging reaction (*i.e.*, the positive electrode of the battery) also involves the OER reaction [31–34]. Hence, OER plays a significant role in the energy field.

Among the many factors affecting electrocatalytic water oxidation, the electrocatalyst is at the core [6,26,35,36]. The key to determining the oxygen production efficiency of the electrocatalyst is its conductivity, and the quantity and the quality of its active sites [37–39]. Specifically, the quality of active sites can be reflected by Gibbs free energy barrier (ΔG) for generating its oxygen-producing intermediate [40–42]. Generally, the lower the ΔG, the better. The most classic OER electrocatalysts are two noble metal-based oxides, *i.e.*, RuO_2 and IrO_2. However, their high prices have severely limited their practical applications, and they will be oxidized to RuO_4 and IrO_3, respectively in an alkaline solution after a long period of working time, and then dissolved in the aqueous solution [43–45]. Therefore, it is the core task of electrocatalytic OER to find inexpensive, efficient, and stable electrocatalysts.

In the past few decades, researchers have developed a series of less-expensive materials such as non-noble transition metal oxides [46,47], sulfides [48,49], selenides [50,51], nitrides [52,53], phosphides [54,55], oxyhydroxides [56,57], hydroxides [58,59], Prussian blue analogues (PBAs) [60,61]. However, many shortcomings such as weak conductivity, few active sites, and poor quality of ac-

* Corresponding author.
E-mail address: hecx@szu.edu.cn (C. He).

https://doi.org/10.1016/j.cclet.2021.12.001
1001-8417/

tive sites (high ΔG) still limit their practical applications [62–64]. Whereupon, researchers have taken lots of measures to improve their performance.

Among them, the two-dimensional (2D) strategy is one of the most promising tactics. As we know, since graphene was first obtained in 2004, 2D nanomaterials have received extensive attention in scientific area due to their ultra-thin nanostructures and unique physical and chemical properties [65–69]. In detail, compared with bulk materials, 2D nanomaterials have a large quantity of advantages. (1) The specific surface area and the exposed active sites of 2D nanomaterials have improved significantly. (2) Since most of the atoms of 2D nanomaterials are exposed on the surface, it is much easier to form defects, which are conducive to the increase of edge active sites and coordinated unsaturated metal active sites. (3) Ultra-thin 2D nanomaterials usually have merits in electrical conductivity. This is because electrons are mainly transferred within a thin layer for 2D nanomaterials, while bulk materials have both intra-layer transfer and inter-layer transfer. As a result, the interaction between the layers of bulk materials often causes a certain resistance to the electron transfer in a layer, leading to weak conductivity of bulk materials. Besides, among the advantages of 2D nanomaterials over bulk materials, the second and third points are also the edges of 2D nanomaterials over other non-2D nanomaterials, which is because the ultra-thin and ultra-large 2D nanomaterials cannot only provide a large enough hotbed that is easy to generate defects, but also provide a stable channel within a layer for charge transfer. Therefore, in the past decade or so, a large number of 2D nanomaterials have been applied in the field of electrocatalytic OER [70–77].

Moreover, another very important strategy is the heterometal doping strategy, that is, the bimetallic strategy. Introducing another metal into the original transition metal compound can change the morphology, add defects, change the valence of the original metal, and thus change the quantity and quality of active sites, or even change the location of active sites [35,64,78–85].

It can be seen from the above that combining the 2D strategy and the bimetallic strategy can not only improve the conductivity, but also increase the number and quality of active sites. In particular, when the bimetallic strategy fully improves the activity of the active sites and the 2D strategy fully exposes these active sites on the surface of the material, the synergy between the two strategies can be completely manifested.

Currently, researchers have developed a series of bimetallic 2D nanomaterials for electrocatalytic OER. However, there is no review that specifically summarizes the relevant content on the topic, although some excellent reviews have detailedly discussed the application of 2D nanomaterials in the field [75,77,86–91]. Therefore, in this review, we sum up the electrocatalytic OER application of bimetallic 2D nanomaterials from four aspects: material structure, synthesis method, electrocatalytic performance, and reaction mechanism. The involved materials contain bimetallic 2D metal organic frameworks (MOFs), layer double hydroxides (LDHs), oxides, phosphides, phosphates, PBAs and oxyhydroxides. At the last, we anticipate the development direction and prospect of the field.

2. Materials structure

The transition metal elements in bimetallic two-dimensional nanomaterials are mainly concentrated in the fourth period of the periodic table (the first row of transition metals), which is because the metal elements in this line are cheap and more lively. Among them, the eighth group of iron, cobalt and nickel have similar atomic radii and chemical properties, so they are often utilized to dope with or partially replace each other. Therefore, we often see bimetallic iron-cobalt, iron-nickel or cobalt-nickel two-dimensional materials used in electrocatalytic OER. In addition, OER's bimetallic two-dimensional electrocatalyst also involves other fourth period elements, such as copper, zinc, vanadium and manganese. What is more, it is worth noting that sometimes we can also see the participation of some main group metal elements, such as indium, which is at the fifth period, the third main group. Here, we summarize the structures of representative bimetallic 2D MOF, LDH, oxides, phosphides, and oxyhydroxides as follows.

In the ultrathin NiCo MOF nanosheets prepared by Zhao *et al.* [92], the organic ligand used is benzenedicarboxylic acid (BDC). As shown in Fig. 1a, the statuses of nickel and cobalt are equal in the material structure. They all coordinate with the six oxygen atoms from hydroxyl groups and carboxyl groups to form a virtual octahedral structure. However, on the surface of the two-dimensional MOF, due to the limited growth, some metal atoms have only five coordination bonds, which is the so-called unsaturated coordination state, thus forming a virtual tetragonal pyramid structure. Coordination unsaturated metal atoms are extremely significant in catalytic reactions because they are easily combined with solvents or reactant molecules and become active sites for catalytic reactions.

Most of the bimetallic two-dimensional MOFs are similar to the above-described NiCo MOF nanosheets, that is, the two metals have equal positions and form a *pseudo*-octahedral structure with coordination atoms, and there are many coordination unsaturated metals on the material surface. However, in the MOF prepared by Li *et al.* [93], the bimetallic statuses are unequal. As shown in the Fig. 1b, the bimetallic 2D MOF they prepared is formed with metal phthalocyanine (MPc) as the organic ligand and another metal as the metal junction (Fig. 1b). Therefore, unlike the metal M', the metal M is at the center of the MPc, so the statuses of the two metals differ from each other. As a result, the coordination environment of M is a plane cube composed of four M-N bonds, and that of M' is a plane cube composed of four M-O bonds. The as-synthesized bimetallic MOF nanosheets contain ZnPc-Ni and NiPc-Zn. It is worth noting that because phthalocyanine is a compound with a large conjugated system of 18 electrons, the as-fabricated materials have good conductivity.

Like most bimetallic two-dimensional MOFs, the positions of the two metals are also equal in LDH. In the NiFe LDH prepared by Wang *et al.* [94], both Ni and Fe are connected to six oxygen atoms, so that the metal and the coordinated oxygen atoms form an octahedral structure (Fig. 1c). Besides, similar structures also exist in oxides and oxyhydroxides. For example, in the bimetallic 2D iron-doped nickel oxide nanosheets prepared by Zhuang *et al.* [95], both nickel and iron are connected with six O atoms to form an octahedral structure (Fig. 1d). In the bimetallic oxyhydroxide nanosheet $Fe_{0.33}Co_{0.67}OOH$ prepared by Ye *et al.* [96], the octahedral coordination structure of FeO_6 and CoO_6 can be found (Fig. 1e). At the same time, there are also CoO_4 tetrahedrons in $Fe_{0.33}Co_{0.67}OOH$ nanosheets. In contrast, in the iron-containing cobalt phosphide synthesized by Hu *et al.* [97], iron partially replaced phosphorus, forming iron-cobalt bonds (Fig. 1f).

To sum up, in most oxygen-containing bimetallic two-dimensional materials, the statuses of the two metals are equal, and they coordinate with six oxygen atoms (MO_6) to form a *pseudo*-octahedral structure. It is reported that this structure of MO_6 may be beneficial to the performance of electrocatalytic OER process.

3. Synthetic strategies

In this review, we discuss the preparation of bimetallic two-dimensional nanomaterials from two aspects: bimetallic synthesis strategy and two-dimensional synthesis strategy. In order to better make readers understand the writing logic of this part, we have specially made the following mind map (Fig. 2).

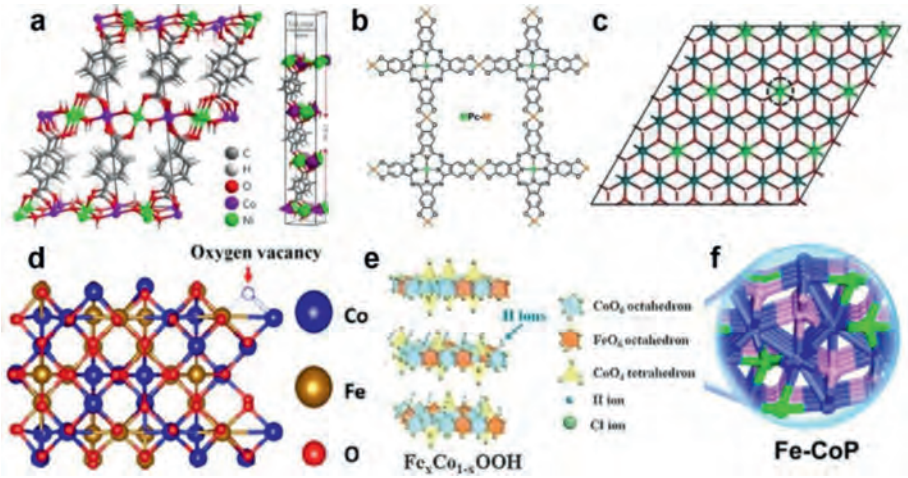

Fig. 1. (a) The bimetallic ultrathin MOF nanosheets formed with benzenedicarboxylic acid (BDC) as the organic ligands and Co and Ni as the metal sites. Reproduced with permission [92]. Copyright 2016, Springer Nature. (b) The conductive 2D MOF formed from metal phthalocyanine (MPc) and metal cations. M and M' stand for two different metal sites. Reproduced with permission [93]. Copyright 2021, Royal Society of Chemistry. (c) 2D NiFe LDH nanosheets. The blue, green, red, and white represent Ni, Fe, O and H atoms, respectively. Reproduced with permission [94]. Copyright 2018, Wiley-VCH. (d) The bimetallic 2D iron-doped nickel oxide nanosheets. Reproduced with permission [95]. Copyright 2018, Springer Nature. (e) The bimetallic oxyhydroxide nanosheet $Fe_{0.33}Co_{0.67}OOH$. Reproduced with permission [96]. Copyright 2018, Wiley-VCH. (f) The iron-containing cobalt phosphide. Green for Fe, blue for Co, and pink for P. Reproduced with permission. Reproduced with permission [97]. Copyright 2018, Elsevier.

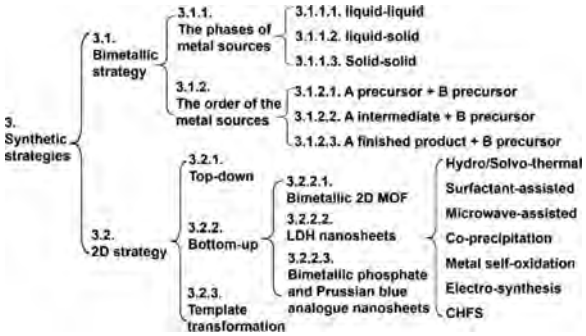

Fig. 2. The mind map of Part 3.

3.1. Bimetallic strategy

3.1.1. The phases of metal sources

From the bimetallic viewpoint, there are two classification routes. According to the phases of the two metal sources, it can be classified as three modes: Liquid-liquid, liquid-solid, and solid-solid. Among them, the liquid-liquid method is the most common one since the homogeneous mixing is more uniform. For example, Zhao *et al.* utilized a mingled solution of $CoCl_2$ and $NiCl_2$ to synthesize ultrathin NiCo bimetallic-organic framework nanosheets [92]. Rosa *et al.* took a mixed aqueous solution of $Ni(NO_3)_2$ and $Fe(NO_3)_3$ as the precursor of the Ni-Fe layered double hydroxide 2D thin films [98]. Liang *et al.* dissolved $FeCl_2$ and $Ni(NO_3)_2$ together into an aqueous solution to prepare Fe-doped $NiPS_3$ nanosheets [72].

Liquid-solid mode is usually taken to directly fabricate the electrode for electrocatlaytic OER. Sun *et al.* prepared bimetallic 2D FeNi MOF by liquid-solid mode (Fig. 3). They dissolved $FeCl_2{\cdot}4H_2O$ and terephthalic acid ($C_8H_6O_4$) in a mixed solution of *N*,*N*-dimethylformamide (DMF)/ethanol/water (14:1:1, v/v/v). After fully stirring, the mixed solution and nickel foam are placed in a Teflon-lined autoclave for solvothermal reaction. In this process, because the $C_8H_6O_4$ solution is acidic, the nickel atoms on the surface of the nickel foam will be partially oxidized to Ni^{2+}, thereby participating in the formation of MOF. Consequently, the FeNi bimetallic MOF nanosheets attached to the surface of the nickel foam can be finally obtained. The advantage of liquid-solid mode is that the as-prepared electrode does not require a binder, and the synthesized bimetallic 2D material can be firmly attached to the surface of the base nickel foam [99].

Pan *et al.* used a very similar method to synthesize FeNi 2D MOF electrodes. However, they utilized $FeCl_3{\cdot}6H_2O$ as the iron source and 2-amino terephthalic acid as the organic ligand. In their synthesis path, Fe^{3+} will oxidize Ni atoms to be Ni^{2+} on the surface of Ni foam, and itself is reduced to Fe^{2+}. Then due to the presence of air in the Teflon-lined autoclave, Fe^{2+} is again oxidized to Fe^{3+}. At last, the metal junctions of the final FeNi MOF nanosheets are still Ni^{2+} and Fe^{3+}. Besides, they took experiments to prove the stability of the bimetallic 2D MOF electrode synthesized *via* solid-liquid mode. After maintaining a current density of 50 mA/cm^2 under applied potential for 24 h, no significant current density loss (<10%) is observed. What is more, they also demonstrated that after the OER reaction, the electrode has undergone a certain change, that is, FeNi MOF nanosheets are partially converted into γ-NiOOH and FeOOH. The former is a highly efficient electrocatalytic OER catalyst, while the latter has poor electrocatalytic performance due to its poor conductivity. However, owing to the direct growth on the Ni substrate, the conductivity of FeOOH is significantly improved, and the OER performance is thus enhanced [100].

Hu *et al.* took a solid-solid metal source model to synthesize two-dimensional Fe-CoP/CoO (Fig. 4) [97]. They directly put the solid metal salts $CoSO_4{\cdot}7H_2O$ and $FeSO_4{\cdot}7H_2O$ in molten sodium hydroxide, and kept the reaction for 1 min to prepare FeCo LDH/CoO. Then they utilized FeCo LDH/CoO as the precursor for phosphating. In detail, FeCo LDH/CoO and NaH_2PO_2 were placed in the same porcelain boat, which were then put into a tube furnace, with NaH_2PO_2 in the upstream position. Afterwards, under the protection of Ar, Fe-CoP/CoO can be obtained after 2 h annealing at 300 °C, while pure Fe-CoP can be acquired within 9 h. In this fabrication method, since molten sodium hydroxide can provide ultra-high concentration of exposed OH^-, which will directly react with Co^{2+} and Fe^{2+} without traditional hydration [101,102], the reaction speed and material quality can be greatly improved. The

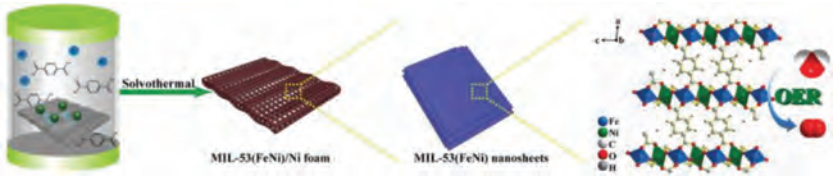

Fig. 3. Schematic illustration of the fabrication of 2D NiFe MOF on nickel foam. Reprinted with permission [99]. Copyright 2018, Wiley-VCH.

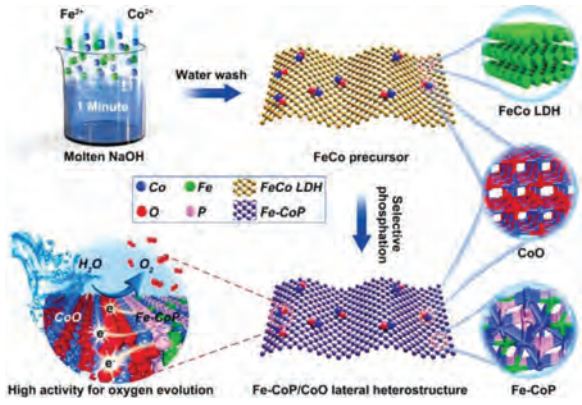

Fig. 4. Schematic illustration of the synthesis of Fe-CoP/CoO nanosheets. Reprinted with permission [97]. Copyright 2021, Royal Society of Chemistry.

FeCo LDH/CoO prepared by this method only takes 1 min, which is much faster than the traditional way [103].

3.1.2. The order of the metal sources

The other classification route from the bimetallic level is based on the orders of the incorporation of metals, which can be divided into three modes: the simultaneous addition of AB precursor, A intermediate + B precursor, and A finished product + B precursor. The first model is the most commonly used one without any particularity, and will not be discussed in detail here.

A intermediate + B precursor: Li *et al.* prepared bimetallic conductive MOF nanosheets (Fig. 5) under the mode of A intermediate + B precursor. They first synthesized monometallic nickel phthalocyanine (NiPc), and then took NiPc (Ni intermediate) and zinc(II) acetate dihydrate (Zn precursor) to fabricate bimetallic 2D MOF (NiPc-Zn) *via* a solvothermal method. In particular, as shown in Fig. 1b, in the NiPc-Zn prepared by this strategy, the statuses of the two metals are unequal. Nickel is located in the center of phthalocyanine, and the coordination environment is Ni-N_4, while zinc is the metal junction connecting NiPc, and the coordination environment is Zn-O_4. As described above in the material structure, due to the 18-electron conjugation in the phthalocyanine, the as-fabricated bimetallic 2D MOF has good conductivity. Besides, they also fabricated ZnPc-Ni using the same synthetic strategy [93].

Li *et al.* exploited the A intermediate + B precursor model to synthesize Fe-Co_3O_4 nanosheets. They first took a simple precipitation method to fabricate 2D Co MOF film on carbon cloth (Co-MOF NS/CC), with $Co(NO_3)_2{\cdot}6H_2O$ as the Co source, 2-methylimidazole ($C_4H_6N_2$) as the organic ligand. Then the prepared Co-MOF NS/CC (Co intermediate) was immersed in the $[Fe(CN)_6]^{3-}$ solution (Fe precursor) and the mixture was stirred for 2 h for anion exchange. After drying, the obtained Fe@Co MOF NS/CC was annealed at 350 °C for 2 h to get Fe-Co_3O_4 nanosheets. In this method, 2D Co-MOF NS assumes the role of a template. The prepared 2D Fe-Co_3O_4 nanosheets have good stability and excellent electrocatalytic OER performance [104].

From the above examples, we can see that the strategy of A intermediate + B precursor can help to obtain 2D nanosheets with inconsistent statuses of two metals. Besides, this strategy always involves with ion-exchange reaction and has certain advantages in preparing products like bimetallic oxide nanosheets that require further calcination.

A finished product + B precursor: Peng *et al.* took the mode of A finished product + B precursor to fabricate a range of bimetallic 2D MOF (Fig. 6). They firstly prepared a 2D Fe-based MOF (HUST-8) with $FeCl_2$ as the iron source and tetrapyridinate as the organic ligand using a diffusion route. Then they employed a reflux means at 85 °C to introduce a single metal atom into the unoccupied porphyrin center of HUST-8 to fabricate bimetallic 2D MOF materials, *i.e.*, Ni@HUST-8, Co@HUST-8, Zn@HUST-8 and Mn@HUST-8. Obviously, in the bimetallic 2D MOF obtained by this method, the positions of the two metals are not the same. Iron assumes the metal joints linking the organic ligands, while the other metal is trapped in the porphyrin center of the ligands. They demonstrated that Ni@HUST-8 has the best OER performance due to the special synergistic effect of Fe and Ni centers. The advantage of this method is that the synthetic temperature is low since the unoccupied porphyrin centers provide appropriate space for external metal ions [105].

Zhou *et al.* reported a cation exchange way to prepare iron-doped $Ni(OH)_2$ and $Co(OH)_2$ nanosheets [106]. This method can also be classified in the model of A finished product + B precursor. Take Fe doped $Ni(OH)_2$ as an example. They put NiOH nanosheets in 50 mL ethanol, and made the solution into a suspension with 3 h of ultrasonication and 1 h of stirring. After that, anhydrous $FeCl_3$ was added, and the mixture was stirred for 12 h at 50 °C to obtain Fe doped $Ni(OH)_2$ nanosheets. The as-fabricated materials had higher electrochemically active surface area (ECSA) and improved surface wettability than that of FeNi LDH prepared by the traditional one-pot method, and thus had higher OER performance. This phenomenon is because that in the process of cation exchange, a chemical etching process occurs simultaneously. In detail, small amount of $FeCl_3$ can be converted into $Fe(OH)_3$ in water, and a little HCl will be produced concomitantly. Consequently, $Ni(OH)_2$ will be partially etched by HCl, resulting in a large number of defects and nanopores.

Like A intermediate + B precursor, A finished product + B precursor also contributes to the synthesis of bimetallic 2D nanosheets with unequal statuses of two metals. Similarly, this strategy often involves ion exchange reactions as well. The difference between the two strategies is that, after the ion exchange reaction, the A finished product + B precursor method directly obtains the final product without further processing such as calcination.

3.2. 2D strategy

From the perspective of synthesizing two-dimensional nanomaterials, there are three strategies, namely top-down, bottom-up and template conversion strategies. Top-down means that the bulk precursor is synthesized first, which is then peeled off into a two-dimensional nanosheet structure by various exfoliation methods. Bottom-up refers to using methods such as solvothermal way to directly prepare 2D nanosheets by controlling reaction conditions

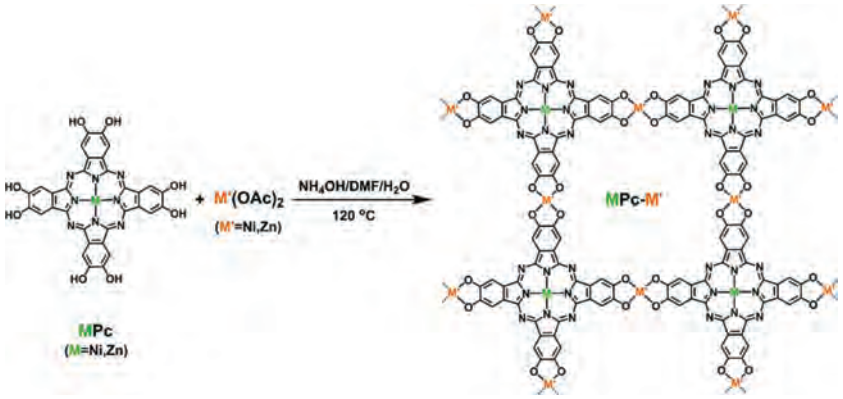

Fig. 5. Schematic illustration of the construction of NiPc-Zn or ZnPc-Ni MOF nanosheets. Reprinted with permission [93]. Copyright 2021, Royal Society of Chemistry.

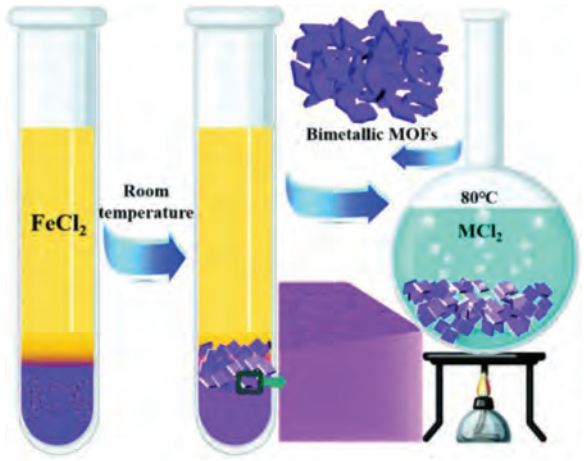

Fig. 6. Schematic illustration of Ni@HUST-8. M stands for metal. Reprinted with permission [105]. Copyright 2020, Royal Society of Chemistry.

and adding modifiers. The template conversion method refers to the use of 2D nanomaterials as precursors and template, which are transformed into new 2D nanomaterials through reactions under certain conditions.

3.2.1. Top-down

Zhao *et al.* employed the top-down strategy to fabricate the ultra-thin NiCo 2D MOF [92]. They first prepared the bulk NiCo MOF using an ultrasound-assisted method. In detail, a mixed solution of DMF, water and ethanol was first prepared in a polytetrafluoroethylene (PE) tube. After that, under the assistance of ultrasound, the ligands, Benzenedicarboxylic acid (BDC), metal sources, $CoCl_2{\cdot}6H_2O$ and $CoCl_2{\cdot}6H_2O$, and triethylamine (TEA) were added to the above solution in turn. After 5-min stirring, the bulk NiCo MOF was initially obtained. Then, after 8 h of strong ultrasonication, ultra-thin NiCo 2D MOF nanosheets were acquired.

It is worth noting that, apart from the above-mentioned case, we have not found more articles concerning the top-down strategy for the preparation of bimetallic 2D MOF nanosheets in recent year literature. This may be attributed to the shortcomings of the top-down way: (1) Due to the stability of the internal structure with interlayer chemical bonds, many bulk MOFs cannot be peeled off, such as MOF-74 [107], zeolitic imidazolate framework-67 (ZIF-67) [108], MOF-5 [109] and Materials Institute Lavoisier (MIL) [110]. (2) Ultrasonic treatment for too long time will inevitably lead to morphological damage and structural deterioration. (3) High-power ultrasound is costly and will produce much noise.

3.2.2. Bottom-up

Bimetallic 2D MOF: Li *et al.* adopted a bottom-up solvothermal strategy to synthesize a series of bimetallic 2D MOFs, including NiFe, NiAl, NiCo, NiMn, and NiCd MOFs [111]. In their scheme, the coordination polymer is restricted from growing in one direction *via* a mixed solution, and the interaction between crystalline layers is successfully inhibited. Specifically, they dissolved the metal salts and the organic ligand (terephthalic acid) in the mixed solution of *N*,*N*-dimethylacetamide (DMAC) and water, and then took a solvothermal reaction to fabricate the above-mentioned bimetallic 2D MOFs. In this process, the configuration of the mixed solvent is the key. Using water alone as the solvent will produce amorphous nanoflowers decorated with nanoparticles, while using DMAC alone will produce fluffy powder. Only when the solvent is the mixture of DMAC and water, can a 2D nanosheet with a good crystal form be produced. Moreover, the output of this route is very large, even reaching gram-level. The nickel-iron metal ion is coordinated with six oxygen atoms (O_6), which come from carboxylate, hydroxyl and water ligands. Metal ions and O_6 form a geometric octahedral structure with the metal ion as the geometric center. These octahedral structures are connected into a chain by ligands, and they are then connected into a network by ligands. The thickness of the 2D MOF is 2–3 coordination layers.

Yang *et al.* took a method very similar to that of Li *et al.* to synthesize CoFe MOF nanosheets and CoNi MOF nanosheets [112]. Different from Li, Yang used 5-((pyridin-4-ylthio)methyl)isophthalic acid as the organic ligands. Therefore, in the 2D MOF they fabricated, the coordination environment of cobalt and iron is four oxygen and two nitrogen atoms, rather than O_6.

Ge *et al.* also successfully synthesized FeCo MOF nanosheets. However, unlike the above method, he added triethylamine (TEA) to the traditional solvent of DMF, ethanol and water, thus eliminating the solvothermal steps, and fabricating the FeCo 2D MOF by simply stirring at room temperature. The ligand they exploited was 1,4-benzenedicarboxylic acid (1,4-BDC) and the metal sources were $Co(NO_3)_2{\cdot}6H_2O$ and $FeCl_3{\cdot}6H_2O$. Herein, without TEA, that is, using the mixture solvent of DMF, ethanol and water, only bulk MOF could be obtained; without water, the final product was merely three-dimensional MOF. Only with the combination solvent of the four liquids, can an excellent two-dimensional MOF structure be obtained. Among the mixture solvent, TEA can not only promote the deprotonation of the carboxylic acid in the ligand, but also accelerate the coordination of the ligand and the metal ion. In the presence of water, a small amount of hydroxide ions from the water can help stabilize the formation of the edge of the two-dimensional material. Compared with bulk materials and three-dimensional materials, the obtained 2D material can significantly improve its electrical conductivity and obtain more unsaturated

metal ligands, thereby efficiently reducing its overpotential. Besides, both Fe^{3+} and Co^{2+} coordinate with O_6, and Fe^{3+} can transfer part of the electrons to Co^{2+} through the ligand, thereby changing the electronic structure of the entire MOF and improving the activity of the catalytic sites [113].

LDH nanosheets: Fan *et al.* utilized a one-step hydrothermal method to synthesize monolayer NiV LDH [114]. They prepared a mixed aqueous solution of $NiCl_2$ and VCl_3, then added a certain amount of urea into the mixture. After transferring the mixture into a Teflon-lined autoclave, they exploited a hydrothermal reaction at 120 °C for 12 h to obtain the final LDH. In this process, weakly alkaline urea provides slow-release OH^-, which is beneficial to the synthesis of thin-layer LDH. The as-prepared monolayer $Ni_{0.25}V_{0.75}$-LDH has electrocatalytic OER activity comparable to NiFe-LDH.

Gong *et al.* used a two-step solvothermal method to adhere NiFe LDH to the outside of multi-walled carbon nanotubes (MWCNT) [115]. They first dispersed MWCNT in anhydrous DMF by ultrasound, and then stirred the mixture vigorously at 85 °C for 4 h. After that, the final product is obtained by two-step solvothermal method (120 °C, 12 h; 160 °C, 2 h).

Jiang *et al.* took a surfactant-assisted solvothermal method to synthesize 2D CoNi LDH on the surface of nickel foam [116]. Typically, they dissolved $Co(NO_3)_2{\cdot}6H_2O$, $Ni(NO_3)_2{\cdot}6H_2O$ and cetyltrimethyl ammonium bromide (CTAB) in a mixed solution of water and methanol. Then the mixture was transferred to a Teflon-lined autoclave, and a piece of nickel foam was partially immersed in the solution. After 24 h of solvothermal reaction (180 °C), NiCo-LDH nanosheet arrays attached to nickel foam were obtained. The strategy of *in-situ* synthesis of 2D LDH directly on nickel foam can avoid the use of binders and conductive additives, and thus can greatly reduce the dead volume of the electrode.

Qiao *et al.* used a one-step microwave-assisted method to synthesize ZnCo LDH nanosheets [117]. They dissolved $Zn(NO_3)_2{\cdot}6H_2O$, $Co(NO_3)_2{\cdot}6H_2O$, and urea in water, and then added ethylene glycol to the solution. After transferring the mixture in a round-bottom flask to the microwave oven, they began the microwave irradiation for 20 min to acquire ZnCo LDH nanosheets. Compared with the hydrothermal method, the microwave-assisted route is more convenient, and the required synthesis time is greatly shortened.

Bera *et al.* took a one-step co-precipitation method to synthesize CoMo LDH nanosheet and nanoflake, respectively [118]. The former was synthesized by using $CoCl_2$ and Na_2MoO_4 solution as the metal source, dropping $NaBH_4$ as the alkali source, and stirring for 20 min. The latter is formed by adding dropwise of a mixed solution of Na_2MoO_4 and NaOH to the $CoCl_2$ aqueous solution and stirring for 15 min. Experimental results proved that the OER activity of CoMo LDH nanosheet is better than that of CoMo LDH nanoflake.

Chen *et al.* synthesized Cu doped cobalt hydroxide (Cu–$Co(OH)_2$) nanosheets *via* a metal self-oxidation method [119]. They first dissolved $CoCl_2$ and $CuCl_2$ in a mixed solution of water and ethanol. Then, under the protection of argon, an ethanol solution of $NaBH_4$ is added to the above solution to reduce Co^{2+} and Cu^{2+} to CoCu alloy particles. After that, the particles were washed and put into water, and after two days of auto-oxidation process in the air, Cu–$Co(OH)_2$ nanosheets were obtained. In addition, they used the same method to synthesize Mn–$Co(OH)_2$ nanosheets.

Li *et al.* synthesized MFe-LDH (M = Ni, Co and Li) on the surface of nickel foam by electrochemical synthesis [120]. Specifically, they took nickel foam as the working electrode, and Pt wire and saturated calomel electrode (SCE) as the counter and reference electrodes, respectively. An aqueous solution of $Ni(NO_3)_2$ (or $Co(NO_3)_2$ or $Li(NO_3)_2$) and $Fe(SO_4)_2$ was used as the electrolyte, and the electrochemical synthesis was conducted at −1 V *vs.* SCE under nitrogen protection and stirring. Then, after auto-

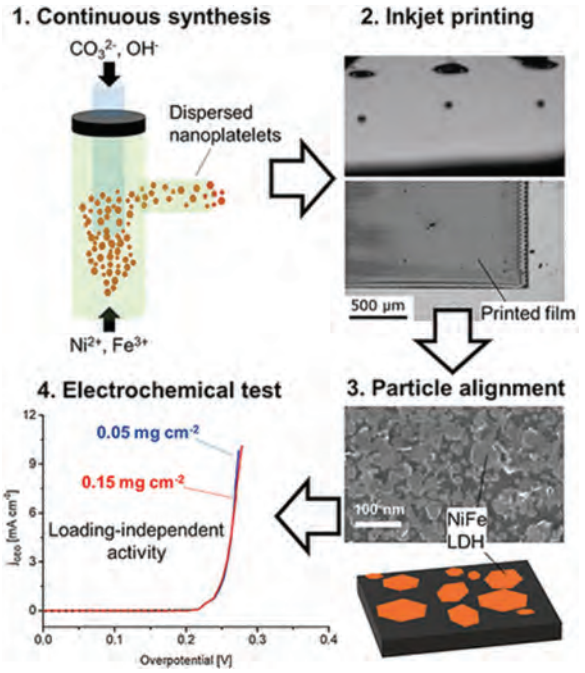

Fig. 7. The fabrication and application of NiFe-LDH nanoplatelets with a continuous hydrothermal flow synthesis (CHFS) method. Reprinted with permission [98]. Copyright 2020, American Chemical Society.

oxidation in the air, MFe LDH containing Fe^{3+} is obtained. It should be noted that during the electrosynthesis process, a reaction of $NO_3^- + H_2O + 2e^- \rightarrow NO_2^- + 2OH^-$ occurs on the surface of the working electrode. The generated OH^- can be combined with metal cations to form LDH.

Rosa *et al.* prepared NiFe-LDH nanoplatelets by the continuous hydrothermal flow synthesis (CHFS) method (Fig. 7) [98]. In brief, they introduced a mixed aqueous solution of KOH and K_2CO_3 at 170 °C from the upper side of the reactor, and another mixed aqueous solution of $Ni(NO_3)_2$ and $Fe(NO_3)_3$ at room temperature from the lower side of the reactor. The mixture obtained after the reaction flowed into a re-heater (80 °C) and stayed for 37 s. Then the obtained products were separated and purified. During the CHFS process, the pressure in the reactor must always be maintained at 200 bar, which is essential for the stability of the flow rate. The CHFS method has the advantages that the reaction conditions are stable and uniform, and stable super-saturation conditions are provided in the material mixing stage, thereby reducing the heterogeneity of the obtained nanomaterials.

It can be seen from the above that bimetallic 2D LDH nanosheets can be synthesized by various methods. We have summarized the advantages and disadvantages of these methods in Table 1 for reference [121]. In fact, the preparation of bimetallic 2D LDH is essentially a process of making a weak base from a strong base. The bimetals mentioned in this review contain either cobalt or nickel. Generally, most of the cobalt and nickel salts used are chlorides or nitrates with good solubility, and sometimes acetate is also utilized. For V, Mo, and other non-group-VIII transition metals, we often use vanadate, molybdate, or like as precursors. The alkali taken includes sodium hydroxide (potassium hydroxide), sodium borohydride and urea (from strong to weak). Actually, the methods listed in Table 1 are the conditions required for the reaction, including temperature, pressure, electric field (electrodeposition) and electromagnetic field (microwave). The key to preparing bimetallic 2D LDH is to select suitable precursors, alkali sources, and reaction conditions, so that a sufficiently thin 2D nanosheet can be ob-

Table 1
The advantages and disadvantages of bimetallic 2D LDH synthesis methods.

Methods	Advantages	Disadvantages
Hydrothermal/Solvothermal	Simple equipment	Long reaction time, high temperature
Surfactant-assisted	High-quality	Residual surfactant
Microwave-assisted	Short reaction time	Difficulty in scale-up [121]
Co-precipitation	Short reaction time, mild reaction conditions	Low quality
Metal self-oxidation	Mild reaction conditions	Ultra-long reaction time
Electro-synthesis	Mild conditions, short reaction time	Only suitable for electrode synthesis
Continuous hydrothermal flow synthesis	Uniform and high-quality products	Complex and expensive equipment

tained. For how to choose reaction conditions or reaction methods, Table 1 can be referred to.

Bimetallic phosphate and Prussian blue analogue nanosheets: Han *et al.* synthesized 2D amorphous Fe-doped indium phosphate nanosheets by combining two-phase colloid and solvothermal methods [122]. They first dissolved $In(NO_3)_3{\cdot}4.5H_2O$ and $Fe(NO_3)_3{\cdot}9H_2O$ in oleylamine (OM) and 1-octadecene (ODE) oil solvents to obtain solution A. Then the NaH_2PO_4 aqueous solution was poured into solution A. After mixing, the mixed solution was transferred to a teflon-lined autoclave, and solvothermal reaction was carried out at 180 °C for 24 h. In the process, the oil phase and the water phase are located at the upper and lower parts of the reactor, respectively. The chemical reaction occurs at the interface of the oil phase and the water phase, which is the key to ensuring that the synthesized two-dimensional material is sufficiently thin and amorphous.

Wang *et al.* used a two-step method to synthesize 2D S-CoFe-PBA/carbon fiber paper (CFP) [123]. In the first step, they slowly poured the aqueous solution of $Na_2Fe(CN)_5NO{\cdot}2H_2O$ into the aqueous solution of $Co(NO_3)_2{\cdot}6H_2O$. Then added CFP to the mixed solution and let it stay for 24 h to obtain CoFe-PBA/CFP. In the second step, they took a solvothermal method to prepare S-CoFe-PBA/CFP. In brief, they put thioacetamide (TAA) and CoFe-PBA/CFP in ethanol and transferred the mixture to a Teflon-lined autoclave, and then kept it at 90 °C for 1.5 h.

3.2.3. Template transformation

Yao *et al.* transformed FeCo oxide nanosheets into 2D FeCo MOF *via* a solvothermal method. They first synthesized FeCo bimetallic nanosheets, then placed them in a mixed solvent of DMF, water and ethanol, and added the ligand 2,5-dihydroxyterephthalic acid to convert the oxide into a two-dimensional MOF in a Teflon-lined autoclave (80 °C, 12 h). The 2D MOF prepared by this method is very thin, only 2.6 nm, thanks to its ultra-thin precursor (FeCo oxide nanosheets, 1.2 nm). In the process, the precursor serves as a template, which can limit the growth of MOF only on a two-dimensional plane, instead of longitudinal direction. Besides, no need for surfactants is another advantage. The resulting product has an overpotential of 298 mV for electrocatlaytic OER. In particular, it has an ultra-low Tafel slope, only 21.6 mV/dec. Unsaturated metal sites are the merits of the 2D FeCo MOF, and the electron transfer from Co^{2+} to Fe^{3+} is a key for the excellent OER performance [124].

Cai *et al.* used a simple ligand-assisted synthesis method to convert the CoFe LDH into 2D CoFe MOF. Specifically, they put CoFe LDH and MOF organic ligand (terephthalic acid) into DMF solvent with ultrasonication, and then took solvothermal means to transform LDH into 2D MOF. In the process, LDH can continuously provide metal ions, and its 2D structure serves as a template for generating 2D MOF. Besides, their experimental results proved that the product obtained by the precursor conversion method is more catalytically active than that acquired from the traditional top-down or bottom-up synthesis routes [125].

Zhang *et al.* took the template transformation way for the fabrication of LDH. They first synthesized 2D FeNi MOF on the surface of Cu foil [126]. In brief, they placed the Cu foil in the mixed solution of potassium(III) trihydrate trioxalate (Fe source), $NiCl_2{\cdot}6H_2O$ (Ni source) and tetrapentyl ammonium bromide (organic ligand). After staying for 10 min, the Cu foil was taken out, washed and dried, and a 2D FeNi MOF supported on the Cu foil (FeNi MOF/Cu) was obtained. Then they placed FeNi MOF/Cu in water and added potassium hydroxide solution dropwise to the water. After 30 min, the 2D MOF was completely converted to 2D LDH. After washing and drying, 2D FeNi LDH/Cu foil was obtained. They also obtained FeCo LDH/Cu foil using the same method, and some other 2D trimetal FeNiCo LDH/Cu foil.

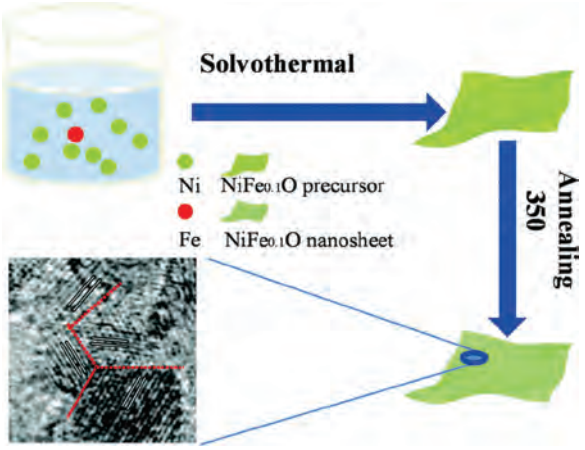

Fig. 8. Schematic illustration of the synthesis of NiFe oxides. Reprinted with permission [127]. Copyright 2020, Royal Society of Chemistry.

Dong *et al.* converted 2D NiFe LDHs into two-dimensional NiFe oxides by calcination (Fig. 8) [127]. They first synthesized 2D NiFe LDH by solvothermal method. In particular, they chose polyethylene glycol 200 (PEG-200) as the solvent. PEG-200 is a good morphology control agent, and can control the formation of nanostructures. This is because the two hydroxyl groups of PEG-200 can be selectively adsorbed on certain surfaces to promote the growth rate of these surfaces. Typically, they took $Ni(NO_3)_2{\cdot}6H_2O$ and $Fe(NO_3)_2{\cdot}9H_2O$ as the metal sources, and anhydrous sodium acetate (CH_3COONa) as the alkali source, and fully dissolved the three in PEG-200. Then the solvothermal reaction was carried out at 200 °C for 16 h. After drying, 2D NiFe LDH nanosheets were obtained, which was then annealed at 350 °C to obtain Fe doped NiO nanosheets. In the transformation process (annealing), NiFe LDH assumes the role of template and the precursor of Fe doped NiO nanosheets.

Li *et al.* used 2D Fe@Co-MOF as a template and calcined it to obtain 2D Fe-Co_3O_4 [104]. They first synthesized Co MOF nanosheets on the surface of carbon cloth (Co-MOF NS/CC) by a simple precipitation method. The Co source taken was $Co(NO_3)_2{\cdot}6H_2O$, and the organic ligand was 2-methylimidazole ($C_4H_6N_2$). Then Co-MOF NS/CC was immersed in $[Fe(CN)_6]^{3-}$ solution for 2 h to obtain Fe@Co-MOF NS/CC. After heating at 350 °C

Table 2
Electrocatalytic OER performance of bimetallic 2D MOF nanosheets.

Catalysts (metal and organic ligand)/ thickness	Publishing year	Metal ratio	Electrolyte	Overpotential (mV)@10 mA/cm^2	Tafel slope (mV/dec)	TOF (s^{-1})	Stability	Substrate	Ref.
Co-Cu TCPP/rGO	2019	-	1 mol/L KOH	396	58	-	10 h/1.61 V	Glassy carbon	[131]
FeCo 1,4-BDC/2.2	2021	1:2	1 mol/L KOH	238	52	-	13.9 h/1.49 V	Glassy carbon	[113]
FeCo BDC/5-7	2020	1:2	1 mol/L KOH	274	46.7	-	70 h/10 mA	Glassy carbon	[125]
FeCo H_2L	2020	1:1	0.1 mol/L KOH	355	49.05	0.081/1.63 V	15 h/20 mA	Glassy carbon	[112]
FeCo H_4dobdc/2.6	2019	1:1	0.1 mol/L KOH	298	21.6	-	2.78 h/1.53 V	Glassy carbon	[124]
NiCo MI	2021	5:100	1 mol/L KOH	310	106.3	-	12 h/1.5 V	unknown	[132]
NiCo BDC/3.1	2016	1:1	1 mol/L KOH	250	42	0.86/1.53 V	200 h/1.48V	Glassy carbon	[92]
NiCo BDC/3.1	2016	1:1	1 mol/L KOH	189		-	-	Cu foam	[92]
NiFe NH_2-H_2BDC/10	2020	-	1 mol/L KOH	258@50	40.8	-	24 h/50 mA	Ni foam	[100]
Ni-Fe TPD/100	2020	1.23:1	1 mol/L KOH	240	60.8	0.722/1.53 V	7 h/10 mA	Glassy carbon	[105]
Ni-Fe 1,4-BDC/2	2019	10:3	1 mol/L KOH	221	56	-	20 h/10 mA	Glassy carbon	[111]
NiFe BDC	2019	3:1	0.1 mol/L KOH	310	43.7	-	11 h/10 mA	Glassy carbon	[133]
Fe BDC@Ni BDC/5.5	2018	3.5:1	1 mol/L KOH	265	82	-	-	Glassy carbon	[134]
NiFe TPA/32	2018	-	1 mol/L KOH	233@50	31.3	0.010/1.46 V	4.4 h/100 mA	Ni foam	[99]

Note: CuTCPP stands for copper(II) meso-tetra(4-carboxyphenyl) porphyrin. 1,4-BDC for 1,4-benzenedicarboxylate. BDC for benzenedicarboxylic acid. H_2L for 5-((pyridin-4-ylthio)methyl)isophthalic acid. H_4dobdc for 2,5-dihydroxyterephthalic acid. MI for 2-methylimidazole. NH_2-H_2BDC for 2-amino terephthalic acid. TPD for tetrapyridinate ligand. TPA for terephthalic acid.

for 2 h in the air, Fe-Co_3O_4 nanosheets supported on carbon cloth were obtained.

Chavi *et al.* synthesized $CoFe_2O_4$ and $NiFe_2O_4$ nanosheets through the way of precursor template conversion [128]. They first took a wet chemical route to fabricate CoFe hydroxide. Specifically, they added urea and glucose to a mixed solution of $Co(NO_3)_2{\cdot}6H_2O$ and $FeSO_4{\cdot}7H_2O$. After thoroughly stirring, a solvothermal process was conducted at 140 °C for 6 h to obtain soft black CoFe hydroxide. The $CoFe_2O_4$ nanosheets were acquired after the calcination of CoFe hydroxide at 500 °C for 10 h. The same method was utilized to obtain $NiFe_2O_4$ nanosheets. In this fabrication route, glucose played the role of carbon source and can be used as the template for generating the 2D products. In the subsequent calcination process, the carbon template could be removed.

Jiang *et al.* prepared bimetallic CoFe phosphide ($Co_{1-x}Fe_xP$) ultra-thin nanosheets by a two-step conversion route [129]. They first prepared $Co_{1-x}Fe_x(CO_3)_{0.5}(OH){\cdot}0.11H_2O$ nanosheets using a surfactant-assisted solvothermal method. In the process, they took cobalt acetate and iron acetate as metal sources, CTAB as a surfactant, and the reaction was realized in a mixed solvent of water and ethanol at 180 °C for 24 h. After that, $Co_{1-x}Fe_x(CO_3)_{0.5}(OH){\cdot}0.11H_2O$ was calcined at 320 °C for 5 min to obtain $Co_{3-3x}Fe_{3x}O_4$. Then, in a tube furnace, $Co_{3-3x}Fe_{3x}O_4$ was converted to $Co_{1-x}Fe_xP$ ultra-thin nanosheets with NaH_2PO_2 as P source at 300 °C for 2 h under the protection of argon. It is worth noting that the material had both a crystalline phase and an amorphous phase, and this structure might be beneficial to electrochemical catalytic activity [130].

In summary, the bimetallic 2D MOF and LDH can be transformed into each other, while bimetallic 2D oxides generally need to be converted from LDH by calcination, and phosphides need to be obtained by phosphating LDHs or oxides.

4. Performances

The two most important parameters that characterize the performance of electrocatalytic OER are overpotential and Tafel slope. Overpotential (η) generally refers to the difference between the potential (*vs.* RHE) required to reach a certain current density and the hydrolysis potential (1.23 V *vs.* RHE). In the literature, the overpotential with a current density of 10 mA/cm^2 is usually used as a reference for parallel comparison. The Tafel slope is employed to reveal the electrocatalytic kinetics and activity mechanism, and the smaller the Tafe slope, the faster the reaction kinetics rate. For the specific calculation methods of the two, please refer to the review [45] by Lv *et al.*

In this review, we have listed the relevant results of bimetallic two-dimensional nanomaterials in Tables 2–4. It can be observed from Table 2 [92,99,100,105,111–113,124,125,131–134] that the lowest overpotential of the bimetallic two-dimensional MOF is 189 mV@10 mA/cm^2. It needs to be noted that this value is realized when Cu foam is the substrate. When glassy carbon electrode serves as the base material, the lowest overpotential is 221 mV, which is achieved by the classic bimetallic 2D MOF:NiFe-MOF with 1,4-benzenedicarboxylate as organic ligands. The thickness of the two-dimensional NiFe MOF is only 2 nm, and the bimetallic ratio is Ni:Fe = 10:3. Besides, the lowest Tafel slope of the bimetallic 2D MOF is only 21.6 mV/dec, which is realized by the 2D FeCo MOF with 2,5-dihydroxyterephthalic acid as organic ligands. The thickness of the MOF is 2.6 nm, and the molar ratio of Fe:Co is 1:1.

From Table 3 [94,98,106,114–120,135–140], we can know that the smallest overpotential and the smallest Tafel slope are focused on NiFe LDH, with the thickness of 3 nm, and the NiFe ratio of 6:1. We need to pay attention to the fact that this NiFe LDH has been amorphized and it is foreseeable that amorphization may be a direction to improve OER activity in the future.

In Table 4 [72,95,97,104,118,122,123,128,129,141–143] are 2D oxides, phosphides and Prussian blue analogues, some of which also have a very unmissable potential and Tafel slope, such as $Fe_1Co_1O_x$ with a thickness of only 1.2 nm, and $Co_{0.7}Fe_{0.3}P$ supported on carbon nanotubes.

In addition, some scholars believe that the mass activity, which is the current density per unit mass of a catalyst at a certain potential, can more truly reflect the catalytic ability of the electrocatalyst. However, because there is no uniform standard for the selected specific potential, the concept of mass activity has not yet been widely applied. It may be an essential catalytic performance parameter in the future. Turnover frequency (TOF) refers to the number of times that a unit mole of metal atoms participates in the reaction per unit time (within per second) under a specific potential or current. Its calculation method can refer to the previous literature [144]. However, TOF is also difficult to use for a wide range of lateral comparisons because researchers use different specific potentials or currents.

Moreover, there are two ways to characterize the stability of the catalyst. One way is to compare the polarization curves before and after a certain number of CV cycles (*e.g.*, 1000). The other is to test the lasting time under a certain current or voltage. After comprehensive comparison of Tables 2–4, we found that both FeCo-BDC MOF and NiCo-BDC MOF have reached ultra-long-time curve, indicating that BDC-related MOF might be quite stable. Besides that,

Table 3
Electrocatalytic OER performance of 2D LDH.

Catalysts/thickness (nm)	Publishing year	Synthesis strategy	Metal ratio	Electrolyte	Overpotential (mV)@10 mA/cm^2	Tafel slope (mV/dec)	Mass activity (A/g)	TOF (s^{-1})	Stability	Substrate	Ref.
CoMn-LDH/2.17	2021	Metal oxidation	8:2	1 mol/L KOH	307	86			20 h/20 mA	Nickel foam	[135]
CoMo-LDH/2.5	2020	Co-precipitation	1:0.34	0.1 mol/L KOH	377	41.88		0.008/1.58 V	24 h/10 mA	Glassy carbon	[118]
CoMn-LDH/CNT/7	2016	Co-precipitation	5:1	1 mol/L KOH	300	73.6		0.472/1.58 V	12.5 h/10 mA	Glassy carbon	[136]
CoMn-LDH/3.6	2014	Co-precipitation	2:1	1 mol/L KOH	324	43		1.05/1.58 V		Glassy carbon	[137]
CuCo-LDH	2017	Metal oxidation	0.32:1	1 mol/L KOH	300	47	46	0.011/1.53 V	36 h/10 mA	Glassy carbon	[119]
NiCo-LDH/35	2015	Solvothermal	6:4	0.1 mol/L KOH	290	113	30.6/1.93 V	0.002/1.65 V	24 h/50 mA	Ni foam	[116]
NiFe-LDH	2020	CHFS	3:1	1 mol/L KOH	270	32				Glassy carbon	[98]
NiFe-LDH/3	2019	Hydrothermal	6:1	1 mol/L KOH	190	31		0.16/1.60 V	10 h/1.48 V	Glassy carbon	[138]
NiFe-LDH/1	2018	Cation-exchange	83:17	1 mol/L KOH	245	61		-	10 h/10 mA	Glassy carbon	[106]
NiFe-LDH/V_{Fe}	2018	Co-precipitation	3:1	1 mol/L KOH	245	70				Glassy carbon	[94]
NiFe-LDH/V_{Ni}	2018	Co-precipitation	3:1	1 mol/L KOH	229	62.9				Glassy carbon	[94]
NiFe-LDH	2016	Co-precipitation	-	Unknown	350	49.05		0.08/1.53 V		Glassy carbon	[139]
NiFe-LDH/8	2015	Electro-synthesis	1.91:1	1 mol/L KOH	224	52.8		0.013/1.53 V	50 h/1.55 V	Glassy carbon	[120]
NiFe-LDH/NGF/50	2015	Co-precipitation	3:1	0.1 mol/L KOH	337	45			3.3 h/1.58 V	Glassy carbon	[140]
NiFe-LDH/CNT/5	2013	Solvothermal	5:1	1 mol/L KOH		31		0.56/1.53 V		Glassy carbon	[115]
NiMn-LDH/CNT/7	2016	Co-precipitation	5:1	1 mol/L KOH	350	83.5		0.173/1.58 V	10 h/10 mA	Glassy carbon	[136]
NiV-LDH	2016	Hydrothermal	3:1	1 mol/L KOH	~300	50	190/1.58 V	0.054/1.58 V	25 h/1.56 V	Glassy carbon	[114]
ZnCo-LDH/2	2015	Microwave	1:2	1 mol/L KOH	540/15 mA	101		0.006/1.63 V	10 h/1.55 V	Glassy carbon	[117]

Note: CHFS stands for continuous hydrothermal flow synthesis. CNT for carbon nanotubes. NGF for nitrogen doped graphene framework. V_{Fe} for Fe vacancies. V_{Ni} for Ni vacancies.

Table 4
Electrocatalytic OER performance of bimetallic 2D oxide, phosphide, phosphate, PBA.

Catalysts/thickness (nm)	Publishing year	Metal ratio	Electrolyte	Overpotential (mV)@10 mA/cm^2	Tafel slope (mV/dec)	Mass activity (A/g)	TOF (s^{-1})	Stability	Substrate	Ref.
Fe-NiO	2020	0.1:1	1 mol/L KOH	274	79.1			10 h/10 mA	Glassy carbon	[118]
Fe-Co_3O_4	2019	0.25:1	1 mol/L KOH	290	67.9			25 h/10 mA	Carbon cloth	[104]
$CoFe_2O_4$/50	2018	1:2	1 mol/L NaOH	410	64	31.35			Glassy carbon	[128]
$NiFe_2O_4$/50	2018	1:2	1 mol/L NaOH	460	80	10.68			Glassy carbon	[128]
$Fe_1Co_1O_x$/1.2	2018	1:1	1 mol/L KOH	225	36	233/1.58 V	1.05/1.58 V	2.8 h/28 mA	Glassy carbon	[95]
Fe-CoP/CoO/8-10	2018	1:4	1 mol/L KOH	219	52				Glassy carbon	[97]
$Co_{0.8}Fe_{0.2}P$/2.5	2018	4:1	1 mol/L KOH	270	50		0.021/1.53 V		Glassy carbon	[129]
$Co_{0.7}Fe_{0.3}P$/C/50	2018	7:3	1 mol/L KOH	270	27		0.92	10 h/1.48 V	Glassy carbon	[141]
Fe-$NiPS_3$/16	2018		1 mol/L KOH	256/30 mA	46		0.23/1.5 V	12 h/30 mA	Glassy carbon	[72]
Fe–$InPO_4$/1.75	2020	1:10	1 mol/L KOH	270	46.47			17 h/10 mA	Ni foam	[122]
S-CoFe-PBA/CFP	2020	4:1	1 mol/L KOH	235	35.2			28 h/10 mA	CFP	[123]
CoFe PBA/1.71	2019		0.1 mol/L KOH	337	53		0.613/1.73 V		Glassy carbon	[142]
CoIr oxide/10	2021	1:3.4	0.1 mol/L $HClO_4$		40			13.5 h/1.6 V	TF-RDE	[143]

Note: S-CoFe-PBA/CFP stands for S-treated two-dimensional (2D) CoFe bimetallic PBA grown on CFP. PBA for Prussian blue analogue. TF-FDE for thin-film rotating disk electrode.

most of bimetallic 2D materials can maintain a good current level within a certain period of time, although the overall stability results of them are irregular. After further analysis, it should be noticed that almost all of the studies investigated in this review involve Ni or Co element, which might be a fundamental reason for the good stability of these materials in alkaline solutions. This is because Co or Ni-related materials can often be oxidized to high-valence NiOOH or CoOOH during the electrocatalytic OER process, and both of NiOOH and CoOOH are reported to be good and stable OER catalysts. Actually, this is the advantage of Ni- or Co-related materials over the traditional precious metals Ru or Ir based materials. According to previous reports, Ru- and Ir-related materials are easily oxidized to RuO_4 and IrO_3 in the OER process under alkaline conditions, thereby being dissolved in the aqueous solution and leading to weak stability [43–45]. Therefore, theoretically speaking, the Ni or Co-2D material can help expose more Ni or Co sites, so that it is logically easier to obtain NiOOH and CoOOH for Ni or Co-2D materials. However, since most articles did not compare 2D materials with non-2D materials in terms of stability, it is difficult to make a more accurate summary at this point. We hope that this content can be added in the future studies about the application of bimetallic 2D materials in electrocatalytic OER.

In the tables of this review, we have summarized the above series of performance characterizations. At the same time, we also summarized the thickness of the two-dimensional nanomaterials, the ratio of the bimetal and the year of publication in the table. It can be found from the tables that the thickness of two-dimensional nanomaterials mostly reaches about 1–10 nanometers. As to the use of metals, the three elements of iron, cobalt and nickel dominate more than half of the previous work. The iron-nickel combination is the most frequently exploited one, which is followed by the iron-cobalt combination. The ratio of iron to nickel is usually 3:1. However, the ratio of iron to cobalt is more various, but in most cases, cobalt content is greater than that of iron. The reason is because, usually, nickel and cobalt are the active sites of OER, and the addition of iron enhances the OER activity of nickel or cobalt through the electronic interaction.

At last, we focused our attention on the only article [143] that reported bimetallic 2D nanomaterial for OER reaction in an acidic solution. In this research, CoIr bimetallic 2D nanoframe was prepared *via* a microwave-assisted route, and then the OER test was conducted in a 0.1 mol/L $HClO_4$ electrolyte. The authors pointed out that the 2D nano-frame structure can provide more sufficient active space for reactive molecules. The bimetallic design can optimize the Gibbs free energy of the reaction intermediate on the one hand, thereby reducing the overpotential. On the other hand, it can reduce the amount of precious metal Ir used.

5. Mechanisms

Many characterizations and density functional theory (DFT) calculations have been used to explore the reaction mechanism of bimetallic 2D nanomaterials in electrocatalytic OER. Among them [111], the ECSA can reflect the quantity of active sites, and the electrochemical impedance spectroscopy (EIS) is related to the charge transfer ability of the catalyst. Besides, since the electrocatalytic OER reactions involved in this review are mostly carried out in alkaline solutions, we present the typical reaction steps of electrocatalytic OER under alkaline condition as follows Eqs. 1–4:

$$H_2O + {}^* \rightarrow {}^*OH + H^+ + e^- \quad (1)$$

$${}^*OH \rightarrow {}^*O + H^+ + e^- \quad (2)$$

$$H_2O + {}^*O \rightarrow {}^*OOH + H^+ + e^- \quad (3)$$

$${}^*OOH \rightarrow O_2 + {}^* + H^+ + e^- \quad (4)$$

In the process, the Gibbs free energy of the four reaction equations are ΔG_1 - ΔG_4, respectively. The reaction step corresponding to the maximum of the four ΔG is the rate determination step (RDS). Generally, RDS is the maximum value of ΔG_2 and ΔG_3. It is reported that the valence state of the metal active site has a great influence on the electrocatalytic OER activity, which is a key factor in determining the value of ΔG_{max} [45].

It is worth noting that the formation of the O–O bond in Eq. 3 belongs to the water nucleophilic attack (WNA) mechanism, also known as the acid-base mechanism. Typically, the active site (*) is electrophilic, and the *O obtained by adsorbing O through the double bond is still electrophilic. The nucleophilic water molecules attack the electrophilic oxygen in *O, thereby forming an O–O σ bond, and at the same time destroying a π bond in *O, and finally forming *OOH. Moreover, regarding the formation of O–O bonds, there are also coupling between two metal oxygen/oxyl units (I2M) mechanisms, bimolecular hydroxyl coupling (BHC) mechanisms, intramolecular hydroxyl coupling (IHC) mechanisms, intramolecular oxygen/oxy coupling (IOC) mechanisms, and redox isomerization (RI) mechanisms [145–149]. Whether these O–O bond formation mechanisms exist in bimetallic 2D nanomaterials for OER remains to be explored.

Additionally, we also need to notice that transition metal compounds, especially iron or nickel or cobalt-related materials, are often oxidized into oxyhydroxides, such as NiOOH, CoOOH, and FeOOH, during electrocatalytic OER process. According to previous reports, the electrocatalytic OER activity of those oxyhydroxides

is very impressive. Some studies believe that they are the "true" effective electrocatalytic OER catalysts, and their performance is much better than other materials [150,151]. As to bimetallic 2D nanomaterials, the same oxidation phenomenon occurs. For example, in the 2D FeNi MOF (the ligand is 1,4-BDC) prepared by Li *et al.* [111], after 1000 CV cycles, it can be seen from the XPS data that Ni^{3+} peaks appear, indicating the formation of NiOOH. Similarly, they also discovered the formation of FeOOH. In the 2D NiCo LDH fabricated by Jiang *et al.*, they found that after a period of electrocatalytic OER, the green NiCo LDH nanosheets will turn to brown-black, which implies the formation of NiOOH and CoOOH [116]. Moreover, in the 2D Fe-$NiPS_3$ prepared by Liang *et al.*, Fe doped NiOOH was also generated in the OER process [72].

Afterwards, we will analyze the benefits of bimetallic 2D nanomaterials to the electrocatalytic OER from the perspectives of "2D" and "bimetal", respectively.

5.1. 2D mechanism

Two-dimensional nanomaterials can reduce the resistance of charge transfer and bring a larger electrochemically active surface area compared with bulk counterparts due to their ultra-thin characteristics, and most of the studies have measured EIS and ECSA to prove this viewpoint.

Besides, in terms of two-dimensional MOF, researchers believe that 2D MOF has more unsaturated metal active sites than bulk counterparts, which is beneficial to the OER process. Zhao *et al.* put forward and profoundly proved this point for a ultrathin bimetal 2D NiCo MOF (BDC as organic ligand) nanosheets (NiCo-UMOFNs) [92]. They experimentally demonstrated that the overpotential of NiCo-UMOFNs was reduced from 317 mV to 250 mV, and the Tafel slope decreased from 61 to 42 mV/dec compared to bulk NiCo MOFs. Besides, they logically speculated that due to the partially terminated BDC coordination bonding with surface metal atoms, the ultra-thinning of NiCo-UMOFNs will produce many unsaturated metal sites. Then, the synchrotron radiation-based X-ray absorption spectra (XAS) and corresponding DFT simulation calculations made it clear that NiCo-UMOFNs do have a large number of unsaturated metal sites. In particular, compared with bulk NiCo MOFs, the M-O coordination number of NiCo-UMOFNs has decreased significantly. Additionally, they explained why the unsaturated metal sites are conducive to the OER reaction through partial state density (PDOS) calculations. In detail, the previous literature proves that, within a certain range, the more filled the 3d e_g state of the metal, the more favorable the OER reaction [152]. PDOS proves that the 3d e_g state of the unsaturated coordination metal of NiCo-UMOFNs is more filled than the 3d e_g state of the saturated coordination metal of the bulk NiCo MOFs, so the OER capability of NiCo-UMOFNs is much stronger.

From the above discussions, we can find that the contribution of "2D" to bimetallic 2D nanomaterials lies in the advantages of the 2D structure in conductivity, the number of active sites, and the formation of coordinated unsaturated metal active sites. In particular, the acquirement of coordinated unsaturated metal active sites can be regarded as a unique contribution of 2D structure, which is rarely reported in other structures.

5.2. Bimetallic mechanism

In Zhao's work, they also revealed how the synergy of NiCo bimetals makes the OER efficiency of NiCo UMOFNs greater than that of Ni UMOFNs and Co UMOFNs [92]. First, their calculation results (Figs. 9a and b) show that the ΔG_{max} of the unsaturated Ni site in NiCo UMOFNs is ΔG_3, 1.55 eV, and that of the unsaturated Co site is also ΔG_3, which is 1.54 eV. Besides, the ΔG_{max} of the unsaturated Ni site in Ni UMOFNs is still ΔG_3, 1.63 eV, whereas that of the unsaturated Co site in Co UMOFNs is ΔG_1, 1.77 eV. Obviously, the ΔG_{max} of NiCo UMOFNs is better than that of single-metal-based Ni UMOFNs and Co UMOFNs. Then, the XPS data shows that some electrons are transferred from Ni^{2+} to Co^{2+} through the oxygen of the ligand, and they explained this transfer process *via* crystal field theory. In detail, since the valence band structure of Co^{2+} is $3d^7$ and has high spin, Co^{2+} owns unpaired electrons on the π symmetric (t_{2g}) d orbital, which will interact with O^{2-} through π-donation (Fig. 9c). On the contrary, the π symmetry (t_{2g}) d orbital of Ni^{2+} is completely occupied, and it interacts with the connected O^{2-} through e^-–e^- repulsion. However, for NiCo UMOFNs, O^{2-} in the middle interacts with Co^{2+} *via* π-donation on the one side and has e^-–e^- repulsion interaction with Ni^{2+} on the other side, thus causing part of Ni^{2+} electrons pass to Co^{2+} through O^{2-}. After that, they took electrochemical experiments to demonstrate NiCo UMOFNs perform much better than the mixture of Ni UMOFNs and Co UMOFNs, disclosing that NiCo UMOFNs with electron transfer from Ni^{2+} to Co^{2+} have better electrochemical activity.

Cai *et al.* took a simple ligand-assisted (terephthalic acid) synthesis method to convert the CoFe LDH into 2D CoFe MOF. XPS data display that the presence of bimetals of the MOF causes some electrons from Co^{2+} to be transferred to Fe^{3+} through the π-conjugation produced by the bridged oxygen, so that Co gains a higher valence state, which may be beneficial to the OER reaction [125].

In the NiFe MOF reported by Sun *et al.* (BDC as the ligand), the DFT optimization result is that Ni is five-coordinated and Fe is six-coordinated. Similar to Zhao and Cai's report, XPS data prove that part of the electrons are transferred from Fe^{2+} to Ni^{2+} through the coordination ligand, resulting in higher OER performance [99].

Liu *et al.* synthesized 2D 5% NiCo MOF wtih 2-methylimidazole as the organic ligand. It should be noted that during the synthesis process of ZIF-68 containing no Ni and only Co, small metal particles were produced, and after the addition of Ni, the resulting MOF does not contain nanoparticles. This phenomenon shows that during the synthesis of MOF, the interaction of bimetallic ions is beneficial to resist the formation of metal particle agglomerates. Moreover, the addition of Ni will slightly change the overall bond length and bond angle in the MOF, which may also be one of the reasons that ultimately promote the performance of OER. Besides, the XPS results again show that the addition of Ni can change the electronic structure of Co, thereby increasing the valence state of Co [132].

In the CoCu bimetallic Porphyrin MOF/rGO (rGO for reduced graphene oxide) designed by Meng *et al.*, Cu is embedded in the center of the Porphyrin ligand, and Co is used as the metal node of the MOF. In their proposed reaction mechanism, as shown in Fig. 10, both Cu and Co are the active sites. When the Co^{2+} adsorbed on the hydroxyl group is deprotonated, the released electrons can be transferred to the copper porphyrin center, reducing Cu^{2+} to Cu^+, so that the OER activity of the copper porphyrin center will increase [131].

In the Cu-doped cobalt hydroxide (CuCo LDH) prepared by Chen *et al.*, the results of XPS indicate that the incorporation of Cu promotes the valence of Co to increase to more than 2. Particularly, compared with $Co(OH)_2$, the binding energy of Co $2p_{3/2}$ and Co $2p_{1/2}$ of CuCo LDH increase by 1.28 eV and 0.65 eV, respectively. This change in electronic structure ultimately promotes the enhancement of the electrochemical OER activity of the Co site. They proved this by the fact that CuCo LDH has less ΔG than $Co(OH)_2$ in each step in the DFT calculation [119].

Fan *et al.* prepared NiV LDH, and they found that the introduction of vanadium on the one hand can effectively improve the charge transport ability of the material, and on the other hand can

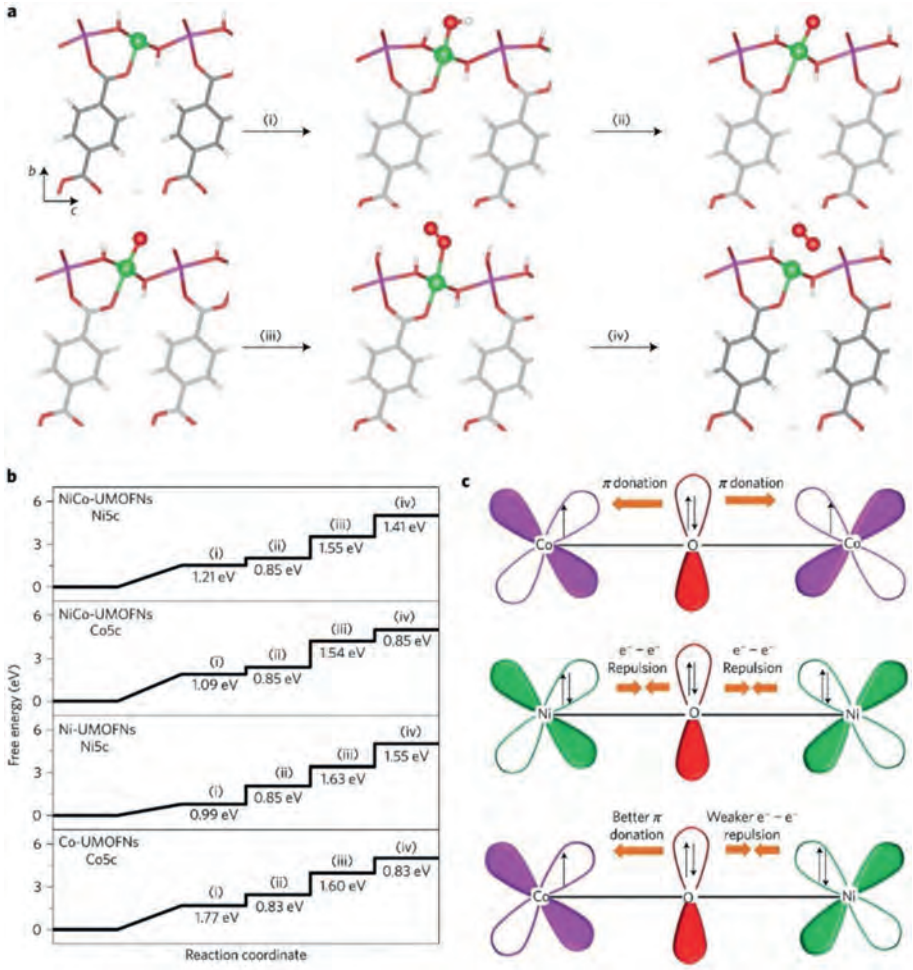

Fig. 9. (a) Electrocatalytic OER steps of UMOFNs. Green for unsaturated metal sites (Ni/Co) coordinated by 5 O atoms, purple for saturated metal sites (Ni/Co) coordinated by 6 O atoms, red for O, grey for C, and white for H. (b) Gibbs free energy of the OER process on UMOFNs surfaces. (c) Schematic illustration of the electronic interaction between Co and Ni in UMOFNs. Reprinted with permission [92]. Copyright 2016, Springer Nature.

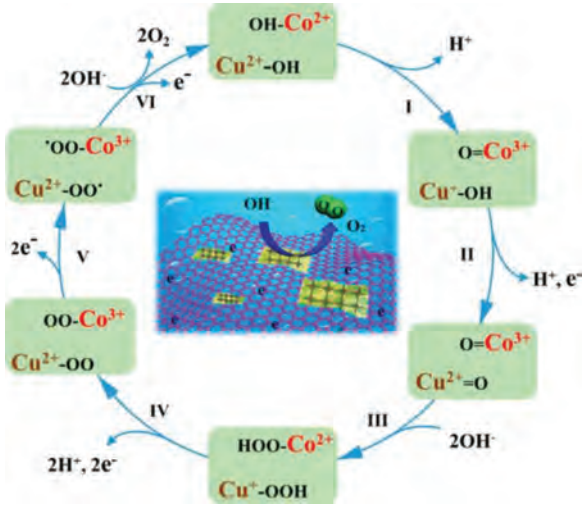

Fig. 10. Schematic illustration of the proposed mechanism for CoCu bimetallic porphyrin MOF/rGO. Reprinted with permission [131]. Copyright 2019, Wiley-VCH.

increase the activity of electrochemically active sites. The Nyquist plots of EIS show that the diameter of $Ni_{0.75}V_{0.25}$-LDH is much smaller than that of $Ni_{0.75}Fe_{0.25}$-LDH, and its charge transfer resistance (R_{ct}) is just 62 Ω cm^2, while $Ni_{0.75}Fe_{0.25}$-LDH is 94 Ω cm^2. Besides, in the DFT calculation, the ΔG_{max} of $Ni_{0.75}V_{0.25}$-LDH is also much smaller than that of $Ni_{0.75}Fe_{0.25}$-LDH [114].

2D Fe-containing cobalt phosphide/cobalt oxide was prepared by Hu *et al.* Through electronic density of states (DOS) calculation they proved that the incorporation of Fe is advantageous to the improvement of the charge transport ability of the material. They compared the DOS (Fig. 11a) and charge distribution (Fig. 11b) of CoP and Fe-CoP, and found that the electronic state of the latter is closer to the Fermi level (refer to the increase in the yellow area in the figure). Obviously, this will facilitate the optimization of OER overpotential and Tafel slope. What is more, they also demonstrated that the ΔG_{max} of Fe-CoPO is 0.07 eV lower than that of CoPO, indicating that the incorporation of Fe is beneficial to improve the OER ability of the compound active sites (Fig. 11c) [97].

Additionally, Liang *et al.* fabricated Fe-doped $NiPS_3$ and calculated the adsorption energy of $NiPS_3$ and Fe-doped $NiPS_3$ for hydroxyl groups (ΔG_{OH}) through DFT calculations (the ΔG_{OH} is also a very important factor in the OER process). Through the optimization of the model, they found that the hydroxyl group will be adsorbed on the phosphorous site, rather than on the metal site. The calculation results display that the ΔG_{OH} of $NiPS_3$ is 1.17 eV, while that of Fe-doped $NiPS_3$ is 1.43 eV. According to previous reports, the best value should be 1.6 eV [153]. Obviously the ΔG_{OH} of Fe-doped $NiPS_3$ is much closer to 1.6 eV, making it clear that the electrochemical activity of transition metal phosphides can be improved by heterometal doping [72].

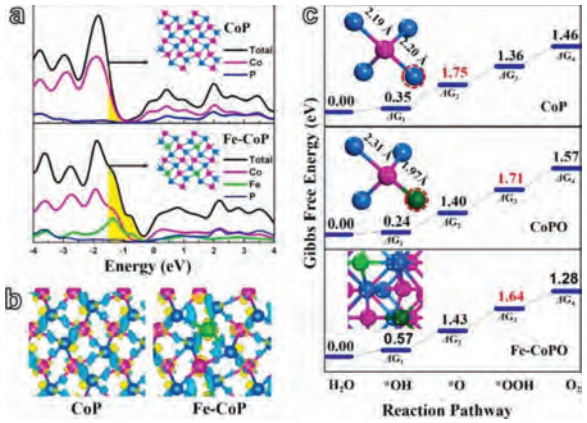

Fig. 11. (a) DOS for CoP and Fe-CoP. (b) The charge density distribution of CoP and Fe-CoP. (c) Gibbs free energy of CoP, CoPO and Fe-CoPO. Purple for Co, blue for P, green for Fe, and dark green for O. Reprinted with permission [97]. Copyright 2018, Elsevier.

In the iron-substituted CoOOH (*i.e.*, $Fe_xCo_{1-x}OOH$) designed by Ye *et al.*, part of the CoO_6 octahedral structure in CoOOH was replaced by FeO_6 octahedrons during the *in-situ* transformation from α-$Co(OH)_2$ to $Fe_xCo_{1-x}OOH$. DFT calculations present that adding Fe into the CoOOH lattice can significantly reduce ΔG_1 ΔG_4, because FeO_6 has a higher OER activity. Besides, $Fe_{0.33}Co_{0.67}OOH$ porous nanosheet arrays grown on carbon fiber cloth (PNSAs/CFC) has high conductivity, high TOF value and large ECSA. Benefiting from the above advantages, $Fe_xCo_{1-x}OOH$ PNSAs/CFC shows greatly enhanced electrocatalytic performance for OER [96].

In short, compared with single-metal 2D nanomaterials, the two metals of bimetallic 2D nanomaterials can help optimize the adsorption energy and Gibbs free energy of the intermediates during OER processes through electron transfer and interaction, thereby improving catalyst activity. In addition, in some cases, bimetallic 2D nanomaterials can also have the effects of improving conductivity and inhibiting agglomeration, which are their advantages over single-metal 2D nanomaterials as well. Moreover, it should be noted that, similar to bimetallic 2D nanomaterials, polymetallic 2D nanomaterials can perform the above-mentioned functions, either. However, because polymetallic materials involve many parameters and the proportion adjustment is more complicated, the optimization difficulty is relatively high. As a result, there are very few reports on the application of polymetallic 2D nanomaterials in electrocatalytic OER. This also highlights the special advantages of bimetallic 2D nanomaterials.

5.3. The synergy of 2D and bimetal effects

To sum up, the two-dimensional characteristics can improve the charge transfer ability of nanomaterials, increase the electrochemical specific surface area and thus increase the quantity of active sites, and can also increase the unsaturated coordination metal sites in the MOF. The characteristics of bimetals can change the electronic structure, thereby improving the quality of active sites. In addition, in some cases, bimetals also contribute to the formation of two-dimensional structures, the improvement of charge transport capabilities, and the increase in the number of active sites. Obviously, when the advantages of the two are combined, the synergy will be manifested. In particular, when the two-dimensional properties improve the electrical conductivity of the material and the number of active sites, and the bimetal enhances the quality of the active sites, the combination of the two can elevate the electrocatalytic OER performance of the material in an all-round way.

6. Summary and outlook

In summary, we reviewed the application of bimetallic 2D nanomaterials in electrocatalytic OER. The materials contain MOF, LDH, oxides, phosphides, phosphates and oxyhydroxides. The metals involved include Fe, Ni, Co from the eighth group and some other elements of the fourth and fifth period, such as Zn, Co, Mn, V and In. From the perspective of bimetals, there are two classifications of the synthesis strategies. One is according to the different states of the metal precursors, and the other is based on the order in which the metal precursors are added. The former has three modes: liquid-liquid, liquid-solid, and solid-solid, while the latter also owns three modes: A precursor + B precursor, A intermediate + B precursor, and A final product + B precursor. When mentioned two-dimensional nanomaterials, the synthesis strategies can be divided into three categories, namely top-down, bottom-up, and template transformation methods. Among them, the top-down way has been seldom used in recent years due to a series of shortcomings. The bottom-up routes contain hydrothermal or solvothermal methods, surfactant-assisted methods, microwave-assisted methods, co-precipitation, metal auto-oxidation, electrochemical methods, CHFS way, ion exchange route, *etc.* As to the template transformation strategy, the bimetallic two-dimensional MOF and LDH can be transformed into each other, while oxides usually need to be converted from hydroxides, and phosphides need to be obtained by phosphating precursors. In regard of reaction mechanisms, the two-dimensional characteristics can mainly increase the charge transport ability and improve the number of electrochemical active sites of the electrocatalyst, while the bimetal can mainly upgrade the quality of the active sites. Therefore, the combination of the two can enhance the electrocatalytic activity of the material in all stages of electrocatalysis.

Although as summarized in this review, the current scientific researchers have made excting achievements in the application of bimetallic 2D nanomaterial for electrocatalytic OER, there are still some sufficiencies that are worthy of our consideration. One is the stability. Although in most of the articles, stability tests have been conducted, few of them compare the stability of bimetallic 2D nanomaterials with non-bimetallic or non-2D nanomaterials, which makes it difficult for readers to understand the special features of bimetallic 2D materials in terms of OER stability. The second point is the acid and neutral test. Judging from the literature in this review, most of the current research on this type of material is concentrated in alkaline solutions, but there are few reports that are under acidic and neutral conditions. Actually, under acidic conditions for water splitting, there are many advantages such as high proton conductivity, high current density, and high energy efficiency. Besides, in the CO_2 reduction reaction, only under neutral conditions, CO_2 will neither be neutralized by alkali, nor will its solubility be reduced by acid. In addition, in the microbial electrolytic cell, neutral conditions are also required to ensure the activity of the microorganisms. Therefore, electrocatalytic OER under acidic or neutral conditions also has great application prospects. However, perhaps since the OER application of bimetallic 2D nanomaterials is in the initial stage, the studies under acidic and neutral conditions are rarely reported, which should be focused on and expanded in the future. Third, as of now, there are no OER reports of bimetallic 2D nanomaterials in pilot application and practical application. However, some of this type of materials have shown high activity and stability in OER, and are even far superior to the performance of existing industrial anode electrodes. With the rapid development of science and technology today, the cycle of a new product from the laboratory to the actual application is also shortening. Therefore, the practical application of bimetallic 2D nanomaterials for OER should also be accelerated.

In addition to the above, the application of relevant materials in electrocatalytic OER can be furtherly promoted from the following aspects: (1) The successful application of bimetallic materials shows that $1+1>2$ effects can be realized between different metals. Therefore, whether the combination of three metals and poly-metals in different proportions can produce good results is worth pondering and exploring. (2) From the viewpoint of two-dimensional materials, there is still much space for improvement in ultra-thinness. In addition, the free superposition of different ultra-thin two-dimensional nanomaterials can form a so-called van der Waals heterojunction which usually has some unique properties. Apparently, it is a great way for future exploring. (3) From the review, we can find that in the bimetallic combination, Fe, Co and Ni are often combined with each other. Among them, the NiFe combination is used the most frequently in the two-dimensional MOF, LDH, oxide, phosphide and oxyhydroxide. Besides, the effect of NiFe combination is also in the highest level. However, the application of NiFe bimetal-based single-atom two-dimensional nanomaterials in the field of electrocatalytic OER has not been reported. Therefore, this is also one of the most worthwhile projects. (4) In new material design and mechanism exploring, DFT calculations are often used to assist in explanation. However, we often find that in some cases, DFT calculation alone is far from enough. Currently, there are applications of finite element calculations in electrocatalysis. For bimetallc 2D nanomaterials, the electron and ion distribution in the unique area between the material edge and the electrolyte will affect the experimental results significantly. The finite element calculation can simulate the specific charge distribution. As a result, the application of this calculation will make the research of bimetallc 2D nanomaterials for OER more powerful and accurate.

Declaration of competing interest

The authors report no declarations of interest.

Acknowledgments

We appreciate the financial support of the National Natural Science Foundation (NNSF) of China (Nos. 21975162, 51902208, 51902209, 22172099), the Natural Science Foundation of Guangdong (No. 2020A1515010840) and Shenzhen Science and Technology Program (Nos. JCYJ20200109105803806, RCYX20200714114535052, RCBS20200714114819161, JCYJ20190808111801674).

References

[1] Q. Hu, Z. Wang, X. Huang, et al., Energy Environ. Sci. 13 (2020) 5097–5103.
[2] Y. Lei, T. Xu, S. Ye, et al., Appl. Catal. B: Environ. 285 (2021) 119809.
[3] Q. Hu, Z. Wang, X. Huang, et al., Appl. Catal. B: Environ. 286 (2021) 119920.
[4] H. Zhang, W. Tian, L. Zhou, et al., Appl. Catal. B: Environ. 223 (2018) 2–9.
[5] H. Zhang, W. Tian, X. Guo, et al., ACS Appl. Mater. Interfaces 8 (2016) 35203–35212.
[6] F. Cao, G. Pan, Y. Zhang, X. Xia, Chin. Chem. Lett. 31 (2020) 2230–2234.
[7] A.S. Huang, G.H. Zhao, H.X. Li, Chin. Chem. Lett. 18 (2007) 997–1000.
[8] X. Li, H. Zhang, Y. Liu, et al., Chem. Eng. J. 390 (2020) 124634.
[9] X. Li, S. Zhao, X. Duan, et al., Appl. Catal. B: Environ. 283 (2021) 119660.
[10] Y. Liu, X. Xu, J. Zhang, et al., Appl. Catal. B: Environ. 239 (2018) 334–344.
[11] J. Zhang, Y. Li, X. Zhao, et al., ACS Nano 14 (2020) 17505–17514.
[12] Q. Hu, G. Li, X. Huang, et al., J. Mater. Chem. A 7 (2019) 19531–19538.
[13] X. Zhao, J. Meng, Z. Yan, F. Cheng, J. Chen, Chin. Chem. Lett. 30 (2019) 319–323.
[14] H. Wang, S. Zhu, J. Deng, et al., Chin. Chem. Lett. 32 (2021) 291–298.
[15] Q. Hu, X. Huang, Z. Wang, et al., J. Mater. Chem. A 8 (2020) 2140–2146.
[16] H. Zhang, W. Tian, Y. Li, et al., J. Mater. Chem. A 6 (2018) 24149–24156.
[17] H. Zhang, W. Tian, X. Duan, et al., Adv. Mater. 32 (2020) 1904037.
[18] H. Zhang, W. Tian, X. Duan, et al., Nanoscale 12 (2020) 6937–6952.
[19] P. Han, T. Tan, F. Wu, et al., Chin. Chem. Lett. 31 (2020) 2469–2472.
[20] C. Wang, L. Jin, H. Shang, et al., Chin. Chem. Lett. 32 (2021) 2108–2116.
[21] Q. Hu, X. Liu, B. Zhu, et al., Nano Energy 50 (2018) 212–219.
[22] B. Zhu, Q. Hu, X. Liu, et al., Chem. Commun. 54 (2018) 10187–10190.
[23] Q. Hu, G. Li, Z. Han, et al., J. Mater. Chem. A 7 (2019) 14380–14390.
[24] Q. Hu, G. Li, Z. Han, et al., Adv. Energy Mater. 9 (2019) 1901130.
[25] X. Li, C. Wang, Y.Y. Liu, et al., Chin. Chem. Lett. 32 (2021) 2239–2242.
[26] L. Jin, H. Pang, Chin. Chem. Lett. 31 (2020) 2300–2304.
[27] Z. Cao, Z. Wang, F. Li, et al., Electrochim. Acta 332 (2020) 135464.
[28] H. Yang, X. Wang, Q. Hu, et al., Small Methods 4 (2020) 1900826.
[29] H. Yang, Q. Lin, Y. Wu, et al., Nano Energy 70 (2020) 104454.
[30] H. Yang, X. Yu, J. Shao, et al., J. Mater. Chem. A 8 (2020) 15675–15680.
[31] G. Li, L. Pei, Y. Wu, et al., J. Mater. Chem. A 7 (2019) 11223–11233.
[32] H. Luo, W.J. Jiang, S. Niu, et al., Small 16 (2020) 2001171.
[33] Y. Guan, N. Li, Y. Li, et al., Nanoscale 12 (2020) 14259–14266.
[34] Y. Sun, Y. Guan, X. Wu, et al., Nanoscale 13 (2021) 3227–3236.
[35] L. Zeng, L. Yang, J. Lu, et al., Chin. Chem. Lett. 29 (2018) 1875–1878.
[36] Y. Li, Q. Guo, Y. Jiang, et al., Chin. Chem. Lett. 32 (2021) 755–760.
[37] X. Li, Y. Wang, J. Wang, et al., Adv. Mater. 32 (2020) 2003414.
[38] L. Zhang, C. Lu, F. Ye, et al., Adv. Mater. 33 (2021) 2007523.
[39] L. Zhang, W. Cai, N. Bao, Adv. Mater. 33 (2021) 2100745.
[40] H. Zhang, C. Li, Q. Lu, M.J. Cheng, W.A. Goddard, J. Am. Chem. Soc. 143 (2021) 3967–3974.
[41] Z. Chen, R. Zheng, M. Graś, et al., Appl. Catal. B: Environ. 288 (2021) 120037.
[42] H. Qiao, H. Liu, Z. Huang, et al., Adv. Energy Mater. 10 (2020) 2002424.
[43] R. Kötz, H. Neff, S. Stucki, J. Electrochem. Soc. 131 (1984) 72–77.
[44] R. Kötz, H.J. Lewerenz, S. Stucki, J. Electrochem. Soc. 130 (1983) 825–829.
[45] L. Lv, Z. Yang, K. Chen, C. Wang, Y. Xiong, Adv. Energy Mater. 9 (2019) 1803358.
[46] S. Cao, J. Qi, F. Lei, Chem. Eng. J. 413 (2021) 127540.
[47] J. Shan, C. Ye, S. Chen, et al., J. Am. Chem. Soc. 143 (2021) 5201–5211.
[48] C. Xuan, W. Lei, J. Wang, et al., J. Mater. Chem. A 7 (2019) 12350–12357.
[49] Y. Zhang, Y. Wang, H. Jiang, M. Huang, Small 16 (2020) 2002550.
[50] Y. Zuo, D. Rao, S. Ma, et al., ACS Nano 13 (2019) 11469–11476.
[51] Y. Guo, C. Zhang, J. Zhang, et al., ACS Sustain. Chem. Eng. 9 (2021) 2047–2056.
[52] C. Liao, B. Yang, N. Zhang, et al., Adv. Funct. Mater. 29 (2019) 1904020.
[53] T. Wu, S. Zhang, K. Bu, et al., J. Mater. Chem. A 7 (2019) 22063–22069.
[54] P. He, X.Y. Yu, X.W.D. Lou, Angew. Chem. Int. Ed. 56 (2017) 3897–3900.
[55] Y. Wang, L. Sun, L. Lu, et al., J. Mater. Chem. A 9 (2021) 3482–3491.
[56] M. Zhou, Q. Weng, X. Zhang, et al., J. Mater. Chem. A 5 (2017) 4335–4342.
[57] L. Yi, Y. Niu, B. Feng, M. Zhao, W. Hu, J. Mater. Chem. A 9 (2021) 4213–4220.
[58] S. Hao, G. Zheng, S. Gao, et al., ACS Sustain. Chem. Eng. 7 (2019) 14361–14367.
[59] H. Meng, W. Xi, Z. Ren, et al., Appl. Catal. B: Environ. 284 (2021) 119707.
[60] Y. Feng, H. Han, K.M. Kim, S. Dutta, T. Song, J. Catal. 369 (2019) 168–174.
[61] X. Gu, Z. Liu, H. Liu, C. Pei, L. Feng, Chem. Eng. J. 403 (2021) 126371.
[62] R. Gao, D. Yan, Adv. Energy Mater. 10 (2020) 1900954.
[63] Y. Xue, Y. Wang, Z. Pan, K. Sayama, Angew. Chem. Int. Ed. 60 (2021) 10469–10480.
[64] S. Li, Y. Gao, N. Li, et al., Energy Environ. Sci. 14 (2021) 1897–1927.
[65] M. Alhabeb, K. Maleski, B. Anasori, et al., Chem. Mater. 29 (2017) 7633–7644.
[66] D. Voiry, H. Yamaguchi, J. Li, et al., Nat. Mater. 12 (2013) 850–855.
[67] B. Radisavljevic, A. Radenovic, J. Brivio, V. Giacometti, A. Kis, Nat. Nanotechnol. 6 (2011) 147–150.
[68] K.S. Novoselov, A.K. Geim, S.V. Morozov, et al., Science 306 (2004) 666–669.
[69] A.K. Geim, K.S. Novoselov, Nat. Mater. 6 (2007) 183–191.
[70] L. Zhao, B. Dong, S. Li, et al., ACS Nano 11 (2017) 5800–5807.
[71] S. Chen, Z. Kang, X. Hu, et al., Adv. Mater. 29 (2017) 1701687.
[72] Q. Liang, L. Zhong, C. Du, et al., Nano Energy 47 (2018) 257–265.
[73] Y. Xu, B. Li, S. Zheng, et al., J. Mater. Chem. A 6 (2018) 22070–22076.
[74] T. Wen, M. Liu, S. Chen, et al., Small 16 (2020) 1907669.
[75] S. Chandrasekaran, D. Ma, Y. Ge, et al., Nano Energy 77 (2020) 105080.
[76] F. Yang, X. Chen, Z. Li, et al., ACS Appl. Energy Mater. 3 (2020) 3577–3585.
[77] J. Yu, F. Yu, M.F. Yuen, C. Wang, J. Mater. Chem. A 9 (2021) 9389–9430.
[78] L. Wang, J. Geng, W. Wang, et al., Nano Res. 8 (2015) 3815–3822.
[79] X. Li, D.D. Ma, C. Cao, et al., Small 15 (2019) 1902218.
[80] J. Du, C. Li, X. Wang, X. Shi, H.P. Liang, ACS Appl. Mater. Interfaces 11 (2019) 25958–25966 f3.
[81] D. Tang, R. Zhao, C. Shen, et al., Electrochim. Acta 324 (2019) 134888.
[82] B.N. Khiarak, M. Hasanzadeh, M. Mojaddami, H. Shahriyar Far, A. Simchi, Chem. Commun. 56 (2020) 3135–3138.
[83] Z. Gao, Z. Yu, Y. Huang, et al., J. Mater. Chem. A 8 (2020) 5907–5912.
[84] Y. Li, Z. Wang, J. Hu, et al., Adv. Funct. Mater. 30 (2020) 1910498.
[85] D. Xiong, M. Gu, C. Chen, et al., Chem. Eng. J. 404 (2021) 127111.
[86] W. Zhang, K. Zhou, Small 13 (2017) 1700806.
[87] Y. Zhou, J. Li, X. Gao, W. Chu, G. Gao, J. Mater. Chem. A 9 (2021) 9979–9999.
[88] X. Lu, H. Xue, H. Gong, et al., Nano Micro Lett. 12 (2020) 86.
[89] J. Zhang, C. Si, T. Kou, J. Wang, Z. Zhang, Sustain. Energy Fuels 4 (2020) 2625–2637.
[90] J. Lei, M. Zeng, L. Fu, Chem. Res. Chin. Univ. 36 (2020) 504–510.
[91] W. Huang, J. Tang, F. Diao, et al., ChemElectroChem 7 (2020) 4695–4712.
[92] S. Zhao, Y. Wang, J. Dong, et al., Nat. Energy 1 (2016) 16184.
[93] J. Li, P. Liu, J. Mao, J. Yan, W. Song, J. Mater. Chem. A 9 (2021) 1623–1629.
[94] Y. Wang, M. Qiao, Y. Li, S. Wang, Small 14 (2018) 1800136.
[95] L. Zhuang, Y. Jia, T. He, et al., Nano Res. 11 (2018) 3509–3518.
[96] S.H. Ye, Z.X. Shi, J.X. Feng, Y.X. Tong, G.R. Li, Angew. Chem. Int. Ed. 57 (2018) 2672–2676.
[97] X. Hu, S. Zhang, J. Sun, et al., Nano Energy 56 (2019) 109–117.
[98] M. Rosa, V.C. Bassetto, H.H. Girault, A. Lesch, V. Esposito, ACS Appl. Energy Mater. 3 (2020) 1017–1026.
[99] F. Sun, G. Wang, Y. Ding, et al., Adv. Energy Mater. 8 (2018) 1800584.

[100] C. Pan, Z. Liu, M. Huang, Appl. Surf. Sci. 529 (2020) 147201.
[101] F. He, X. Deng, M. Chen, Fuel 186 (2016) 605–612.
[102] Z. Hu, X. Xiao, H. Jin, et al., Nat. Commun. 8 (2017) 15630.
[103] J. Yu, Q. Wang, D. O'Hare, L. Sun, Chem. Soc. Rev. 46 (2017) 5950–5974.
[104] Y. Li, W. Zhu, X. Fu, et al., Inorg. Chem. 58 (2019) 6231–6237.
[105] R.L. Peng, J.L. Li, X.N. Wang, et al., Inorg. Chem. Front. 7 (2020) 4661–4668.
[106] Q. Zhou, Y. Chen, G. Zhao, et al., ACS Catal. 8 (2018) 5382–5390.
[107] L.J. Wang, H. Deng, H. Furukawa, et al., Inorg. Chem. 53 (2014) 5881–5883.
[108] J. Qian, F. Sun, L. Qin, Mater. Lett. 82 (2012) 220–223.
[109] J. Li, S. Cheng, Q. Zhao, P. Long, J. Dong, Int. J. Hydrog. Energy 34 (2009) 1377–1382.
[110] K. Guesh, C.A.D. Caiuby, Á. Mayoral, Cryst. Growth Des. 17 (2017) 1806–1813.
[111] F.L. Li, P. Wang, X. Huang, et al., Angew. Chem. Int. Ed 58 (2019) 7051–7056.
[112] C. Yang, C. Yang, W.J. Cai, et al., Catal. Sci. Technol. 10 (2020) 3897–3903.
[113] K. Ge, S. Sun, Y. Zhao, et al., Angew. Chem. Int. Ed 60 (2021) 12097–12102.
[114] K. Fan, H. Chen, Y. Ji, et al., Nat. Commun. 7 (2016) 11981.
[115] M. Gong, Y. Li, H. Wang, et al., J. Am. Chem. Soc. 135 (2013) 8452–8455.
[116] J. Jiang, A. Zhang, L. Li, L. Ai, J. Power Sources 278 (2015) 445–451.
[117] C. Qiao, Y. Zhang, Y. Zhu, et al., J. Mater. Chem. A 3 (2015) 6878–6883.
[118] S. Bera, W.J. Lee, E.K. Koh, et al., J. Phys. Chem. C 124 (2020) 16879–16887.
[119] L. Chen, H. Zhang, L. Chen, et al., J. Mater. Chem. A 5 (2017) 22568–22575.
[120] Z. Li, M. Shao, H. An, et al., Chem. Sci. 6 (2015) 6624–6631.
[121] P. Priecel, J.A. Lopez-Sanchez, ACS Sustain. Chem. Eng. 7 (2019) 3–21.
[122] J. Han, Q. Wei, J. Zhang, J. Mater. Chem. A 8 (2020) 18232–18243.
[123] J. Wang, M. Zhang, J. Li, et al., Dalton Trans. 49 (2020) 14290–14296.
[124] L. Zhuang, L. Ge, H. Liu, et al., Angew. Chem. Int. Ed 58 (2019) 13565–13572.
[125] M. Cai, Q. Liu, Z. Xue, et al., J. Mater. Chem. A 8 (2020) 190–195.
[126] W. Zhang, H. Yu, T. Li, et al., Appl. Catal. B: Environ. 264 (2020) 118532.
[127] Y. Dong, J. Yang, Y. Liu, et al., Dalton Trans. 49 (2020) 6355–6362.
[128] C. Mahala, M.D. Sharma, M. Basu, Electrochim. Acta 273 (2018) 462–473.
[129] M. Jiang, J. Li, J. Li, et al., Nanoscale 11 (2019) 9654–9660.
[130] X. Zhang, J. Zhang, B. Xu, K. Wang, X.W. Sun, Nano Energy 41 (2017) 788–797.
[131] J. Meng, Y. Zhou, H. Chi, et al., ChemistrySelect 4 (2019) 8661–8670.
[132] Q. Liu, J. Chen, P. Yang, et al., Int. J. Hydrog. Energy 46 (2021) 416–424.
[133] Y. Hao, Q. Liu, Y. Zhou, et al., Energy Environ. Mater. 2 (2019) 18–21.
[134] K. Rui, G. Zhao, Y. Chen, et al., Adv. Funct. Mater. 28 (2018) 1801554.
[135] S. Pan, B. Li, J. Yu, L. Zhao, Y. Zhang, Appl. Surf. Sci. 539 (2021) 148305.
[136] G. Jia, Y. Hu, Q. Qian, et al., ACS Appl. Mater. Interfaces 8 (2016) 14527–14534.
[137] F. Song, X. Hu, J. Am. Chem. Soc. 136 (2014) 16481–16484.
[138] S. Jiao, Z. Yao, M. Li, et al., Nanoscale 11 (2019) 18894–18899.
[139] K. Yan, T. Lafleur, J. Chai, C. Jarvis, Electrochem. Commun. 62 (2016) 24–28.
[140] C. Tang, H.S. Wang, H.F. Wang, et al., Adv. Mater. 27 (2015) 4516–4522.
[141] M. Jiang, J. Li, X. Cai, et al., Nanoscale 10 (2018) 19774–19780.
[142] H. Huang, Q. Xue, Y. Zhang, Y. Chen, Electrochim. Acta 333 (2020) 135544.
[143] Y. Ying, J.F. Godínez Salomón, L. Lartundo-Rojas, et al., Nanoscale Adv. 3 (2021) 1976–1996.
[144] P. Tian, Y. Yu, X. Yin, X. Wang, Nanoscale 10 (2018) 5054–5059.
[145] X.P. Zhang, H.Y. Wang, H. Zheng, W. Zhang, R. Cao, Chin. J. Catal. 42 (2021) 1253–1268.
[146] X.P. Zhang, A. Chandra, Y.M. Lee, et al., Chem. Soc. Rev. 50 (2021) 4804–4811.
[147] L. Xie, X.P. Zhang, B. Zhao, et al., Angew. Chem. Int. Ed. 60 (2021) 7576–7581.
[148] X. Li, X.P. Zhang, M. Guo, et al., J. Am. Chem. Soc. 143 (2021) 14613–14621.
[149] Y. Liu, Y. Han, Z. Zhang, et al., Chem. Sci. 10 (2019) 2613–2622.
[150] L. Chen, X.L. Dong, Y.G. Wang, Y.Y. Xia, Nat. Commun. 7 (2016) 11741.
[151] J. Zhang, X.X. Li, Y.T. Liu, et al., Nanoscale 10 (2018) 11997–12002.
[152] J. Suntivich, K.J. May, H.A. Gasteiger, J.B. Goodenough, Y. Shao-Horn, Science 334 (2011) 1383–1385.
[153] C. Kuo, K. Balamurugan, H. Wei, et al., Curr. Appl. Phys. 16 (2016) 404–408.